

# Mineral Lamination Development in Layered Gabbros of the British Palaeogene Igneous Province: A Combined Anisotropy of Magnetic Susceptibility, Quantitative Textural and Mineral Chemistry Study

**BRIAN O'DRISCOLL<sup>1,2\*</sup>, CARL T. E. STEVENSON<sup>3</sup>  
AND VALENTIN R. TROLL<sup>1†</sup>**

<sup>1</sup>DEPARTMENT OF GEOLOGY, MUSEUM BUILDING, TRINITY COLLEGE, DUBLIN 2, IRELAND

<sup>2</sup>SCHOOL OF GEOLOGICAL SCIENCES, UNIVERSITY COLLEGE DUBLIN, BELFIELD, DUBLIN 4, IRELAND

<sup>3</sup>SCHOOL OF GEOGRAPHY, EARTH, AND ENVIRONMENTAL SCIENCES, UNIVERSITY OF BIRMINGHAM, BIRMINGHAM B15 2TT, UK

**RECEIVED APRIL 11, 2007; ACCEPTED APRIL 8, 2008  
ADVANCE ACCESS PUBLICATION MAY 15, 2008**

*Quantitative textural analyses including anisotropy of magnetic susceptibility (AMS) and crystal size distribution measurements were combined with detailed field structural measurements and major element profiling of cumulus plagioclase crystals to study the development of igneous textures in the 'Fluxion Gabbros' of the Ardnamurchan Centre 3 intrusion and the Druim Hain Layered Gabbro, Isle of Skye, both in NW Scotland. Both lithologies studied exhibit mineral lamination (sometimes intensely developed), historically attributed to magma flow at a melt–crystal mush interface. Unlike the Ardnamurchan laminated gabbros, the Druim Hain gabbros lack evidence of sedimentary structures or visible linear alignments of mineral grains on planes of lamination. Syn-magmatic deformation is common in the Ardnamurchan rocks, suggesting movement of unconsolidated cumulate. Plagioclase and clinopyroxene are cumulus in both cases, and magnetite is also cumulus in the Ardnamurchan laminated gabbros. Magnetite occurs as cumulus and intercumulus crystals in the Druim Hain intrusion, in some instances in quantities up to 30 vol. %. Petrographic observation suggests that the Ardnamurchan rocks have undergone a degree of sub-solidus readjustment at grain boundaries. The Druim Hain rocks exhibit an inherited-unmodified impingement texture (with good examples in some cases of melt-present textural equilibrium)*

*although overgrowth on crystals has also occurred in some magnetite-rich samples. Bulk magnetic susceptibilities at both localities are generally  $(10–230) \times 10^{-3}$  (in SI system), consistent with a magnetite-dominated susceptibility. The magnetic foliation in each locality is parallel to the visible mineral lamination in almost all samples. AMS measurements on the Ardnamurchan gabbros reveal that magnetic lineations are oriented confocally around the intrusion; that is, consistently plunging down-dip on lamination planes. These AMS data are supported by plagioclase and magnetite lineation orientations measured by image analysis on thin-sections cut parallel to the mineral lamination. On the other hand, a lack of visible lineations in the Druim Hain rocks is further emphasized by randomly oriented lineations returned by the AMS and image analysis techniques. Crystal size distribution (CSD) and mineral chemical data suggest the presence of a single population of plagioclase crystals at both localities, with evidence of a simpler crystallisation history at Druim Hain. Our combined datasets indicate that the Ardnamurchan fabrics formed in the crystal mush, and have subsequently been affected (mildly degraded) by sub-solidus recrystallization. In contrast, the Druim Hain fabrics may have formed through primary in situ crystallization. Compaction has affected some of the Druim Hain samples, giving rise to solid-state deformation features*

\*Corresponding author. Present address: School of Physical and Geographical Sciences, Keele University, Keele ST5 5BG, UK. Telephone: +44 (0)1782583184. Fax: +44 (0)1782715261.

E-mail: b.odriscoll@esci.keele.ac.uk

†Present address: Department of Earth Sciences, Villavägen 16, SE-752 36 Uppsala, Sweden.

© The Author 2008. Published by Oxford University Press. All rights reserved. For Permissions, please e-mail: journals.permissions@oxfordjournals.org

and a coarser grain size. No correlation is observed between the strength of the AMS fabric and the volume of magnetite present in the Druim Hain gabbros, suggesting that clinopyroxene and plagioclase control the shape of magnetite crystals, and hence the AMS fabrics.

KEY WORDS: mineral lamination; crystal size distribution; layered gabbros; anisotropy of magnetic susceptibility

## INTRODUCTION

Layered mafic and ultramafic intrusions often contain layer-parallel fabrics defined by the planar arrangements of tabular or platy cumulus minerals (mineral lamination). The origin of mineral lamination and magmatic layering in layered intrusions is, however, poorly understood. Some examples of layered rocks exhibit a lineation of crystals on mineral lamination surfaces, or 'sedimentary-type' structures; features that have led to interpretations involving magmatic flow (e.g. Wager & Brown, 1968; Irvine, 1980; Irvine *et al.*, 1998). However, even when present, visible lineations are difficult to measure accurately in the field, and few studies have confidently mapped out consistent magmatic lineation patterns at the intrusion scale (e.g. McBirney & Nicolas, 1997). In the absence of visible lineations, the development of mineral lamination in mafic and ultramafic rocks has been attributed to a wide range of primary and secondary magma chamber processes (see Irvine *et al.*, 1998). The implication of this is that primary flow mechanisms cannot be held exclusively responsible for mineral lamination development in layered rocks.

Studies of magmatic layering in plutonic rocks have incorporated many new quantitative textural and geochemical techniques in recent years as the debate over mechanisms of layer-forming processes and accumulation of crystals in magma chambers continues (e.g. Launeau & Cruden, 1998; Ferré *et al.*, 2002; Higgins, 2002a; Jerram *et al.*, 2003; Holness, 2005; Holness *et al.*, 2007; O'Driscoll *et al.*, 2007a). We have combined structural, petrological and mineralogical data to better understand mineral lamination development in two layered mafic intrusions in the British Palaeogene Igneous Province (BPIP), NW Scotland. These are the Centre 3 Fluxion Gabbros on the Ardnamurchan peninsula and the Druim Hain Layered Gabbro, on the Isle of Skye, both in NW Scotland (Fig. 1a). From the presence of consistently oriented linear arrangements of mineral grains and field evidence for syn-magmatic deformation, we show that mineral lamination in at least one of our study areas can be attributed to the remobilization of unconsolidated crystal mushes. We also provide textural and mineralogical evidence (in agreement with recent studies; e.g. Higgins, 2002a; Boorman *et al.*, 2004; Holness *et al.*, 2007) that textural ripening may modify primary magmatic textures, by highlighting varying ways in which planar and linear alignments of crystals may be affected by postcumulus processes.

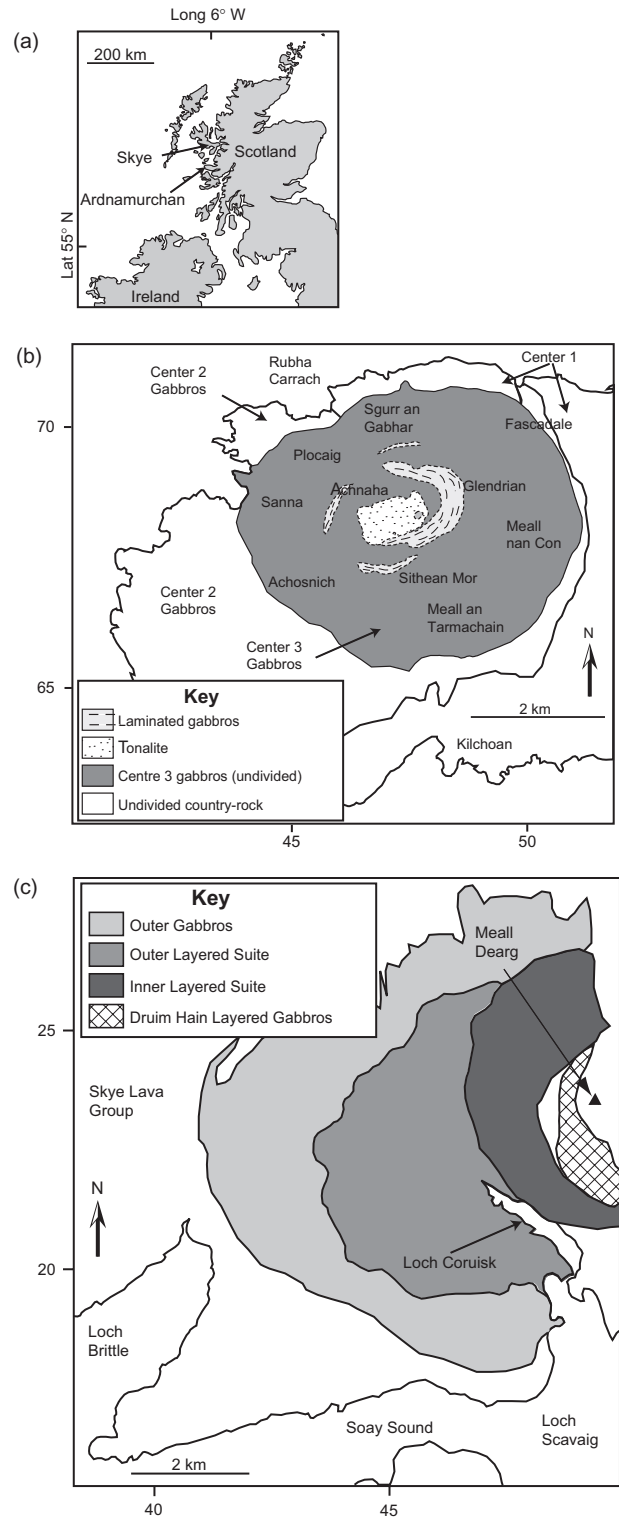


Fig. 1. Regional map of NW Scotland (a) and locality maps for the Ardnamurchan (b) and Skye (c) igneous centres, showing the major lithological units and gabbro bodies of interest in this study.

### Ardnamurchan Centre 3 Gabbros

The igneous central complex of Ardnamurchan has been described as an eroded section through a volcanic complex (Woodcock & Strachan, 2000; Emeleus & Bell, 2005), that hosts three distinct (successive) foci of sub-volcanic intrusive activity (Centres 1, 2 and 3; Richey & Thomas, 1930; Woodcock & Strachan, 2000; Emeleus & Bell, 2005). Centre 3 is dominated by a gabbroic intrusion historically referred to as the Great Eucrite. This body encompasses a suite of smaller, arcuate gabbro bodies; the 'Inner' and 'Biotite' Eucrite ring-dykes, the 'fluxion-gabbro ring-dykes' at Sithean Mor and Glendrian, and several other quartz-gabbro ring-dykes in the Achnaha area (Fig. 1b; Richey & Thomas, 1930). All of these intrusions, together with a late granite body and a net-veined dolerite, have been interpreted as forming part of a single layered intrusion that underwent a significant degree of central subsidence at a late stage in its crystallization history (O'Driscoll, 2007). The gabbros of interest in this paper are the Centre 3 'Fluxion Gabbros' of Richey & Thomas (1930) [or 'laminated gabbros' of O'Driscoll (2007)].

Richey & Thomas (1930) suggested that the planar mineral lamination or 'fluxion structure' of the Centre 3 Fluxion Gabbros resulted from the flow of a crystal mush into a ring-cavity, a theory supported by Bradshaw (1961), Wills (1970) and Fortey (1980). O'Driscoll *et al.* (2006) and O'Driscoll (2007) found that there are four areas of laminated gabbro in Centre 3 (Fig. 1b), that each of these bodies is layered, and that layer planes have a similar (inward-dipping) orientation to those in the Great Eucrite. The latter study reported the absence of chilled margins or intrusive contacts with the surrounding gabbro, and concluded that the laminated gabbros possibly represented two stratigraphically constrained horizons (one comprising the Sithean Mor, Achnaha and Sgurr an Gabhar bodies, and the other the Glendrian body) in a layered mafic lopolith (Fig. 1b). Following O'Driscoll (2007), we refer to the 'fluxion structure' in these rocks as 'mineral lamination', and the 'Fluxion Gabbros' as 'laminated gabbro', to avoid the genetic connotations of flow implied by the former terminology.

### Skye Cuillin Gabbro Complex

The Cuillin Gabbro Complex of Skye (with a diameter of ~8 km) has been subdivided into three major groups; the Outer Gabbros (oldest), the Outer Layered Suite, and the Inner Layered Suite (youngest) (Fig. 1c) (Emeleus, 1991; Emeleus & Bell, 2005). The Inner Layered Series consists of a number of distinct masses of layered and unlayered gabbro, bytownite gabbro and bytownite troctolite. Of these, the Inner Gabbros, also referred to as the Druim Hain layered gabbros (Fig. 1c), exhibit spectacular magmatic layering and layer-parallel mineral lamination (Geikie & Teall, 1894; Harker, 1904; Wager &

Brown, 1968; Emeleus & Bell, 2005). The Druim Hain gabbros are poorly studied, and have not been reinvestigated since the pioneering work by Wager & Brown (1968).

## FIELD OBSERVATIONS

### Ardnamurchan laminated gabbros

The petrology and field relations of the Ardnamurchan laminated gabbros have been described in detail by Richey & Thomas (1930) and O'Driscoll (2007), and are summarized below. These gabbros are characterized by a sometimes intensely developed mineral lamination defined by the planar arrangement of tabular and prismatic plagioclase crystals (Fig. 2a). The mineral lamination in these bodies always strikes parallel to their outer margins and consistently dips toward the centre of the pluton. Fabrics in the outer areas at Sithean Mor, Achnaha and Sgurr nan Gabhar typically dip inward at 50–80° (Fig. 3a). In contrast, dip values of 30–50° are characteristic of the extensive interior arcuate area of laminated gabbro around Glendrian (Fig. 3a). These data, together with observed (mapped) thicknesses of laminated gabbro, indicate approximate structural thicknesses of ≤150 m and ≤250 m for the two groups, respectively. Subtle modal layering associated with (and parallel to) the mineral lamination is frequently present, defined by relatively enriched bands of plagioclase or clinopyroxene. Small-scale structures that are interpreted as evidence for syn-magmatic deformation in the laminated gabbros are common; for example, boudinaged layers and slumped and intricately churned-up crystal slurries (Fig. 2b and c). Sedimentary structures such as modally graded bedding and load structures are also present in the laminated gabbros, although they are not common. No evidence of crystal-plastic deformation is observed with this planar fabric and only rarely can visible lineations be distinguished on mineral lamination surfaces.

### Druim Hain layered gabbros

The layered gabbros exposed on the Druim Hain ridge comprise a sequence of layered cumulates ~700 m thick. Layering is poorly developed with no evidence of an associated mineral lamination observed at the base of the intrusion (lowermost 250 m of stratigraphy is in the west and NW). Above this is ~400 m of superbly well-layered, well-laminated gabbro, comprising olivine, plagioclase, clinopyroxene and magnetite-rich layers.

Monomineralic layers are rare; orthocumulate layers rich in one or two mineral components (usually plagioclase or clinopyroxene) are more typical. Modal layering generally occurs at a scale of centimetres to metres (Fig. 2d). There is no evidence for cyclic or rhythmic repetition of sequences or packages of magmatic layers up sequence, although the layered sequence described above is punctuated by five thin plagioclase-rich layered

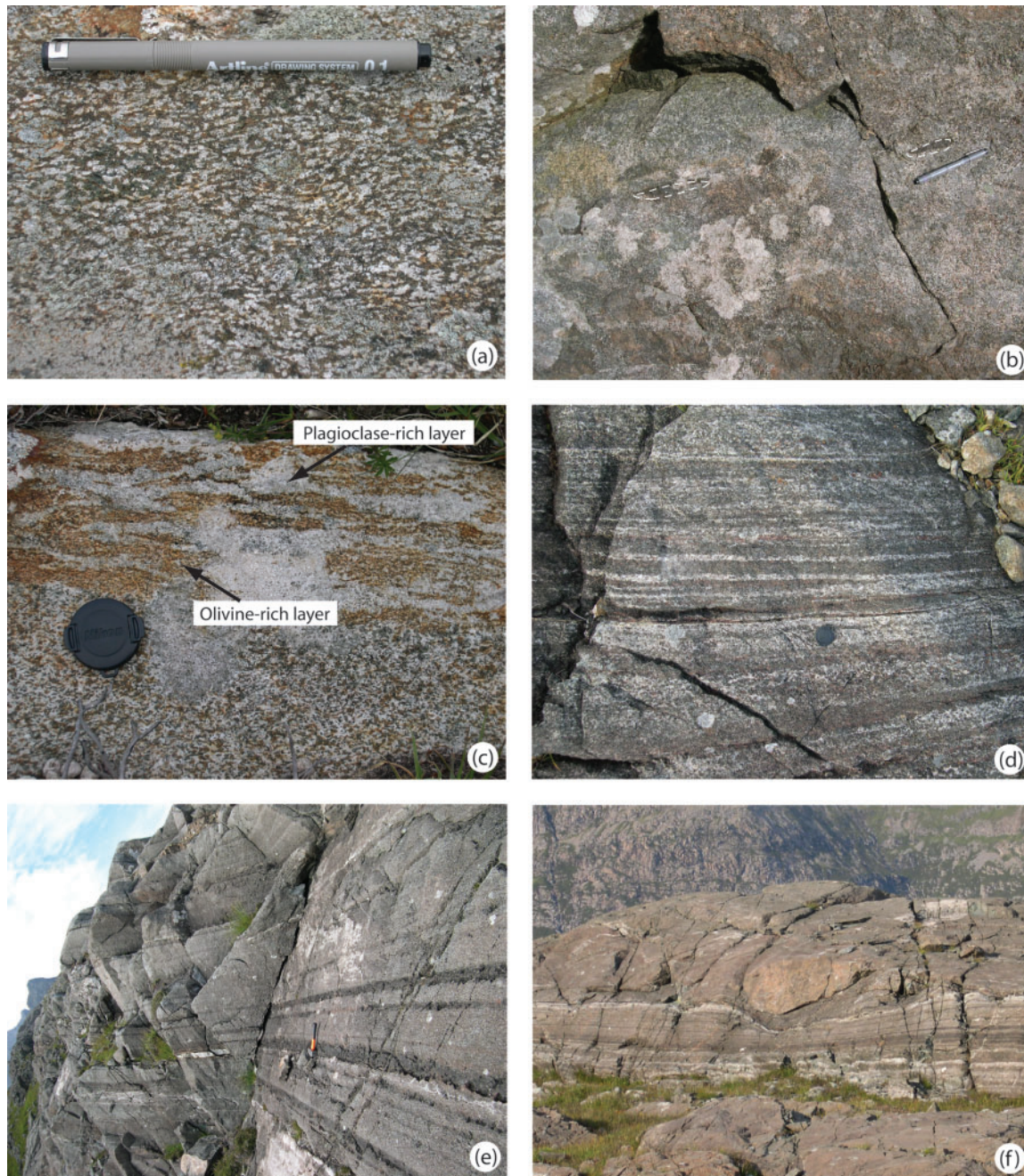


**Fig. 2.** (a) Mineral lamination of plagioclase in the Achnaha laminated gabbro (adapted from O'Driscoll *et al.*, 2006). (b) Syn-magmatic boudinage structure in a pyroxene-rich layer (highlighted) in the laminated gabbro at Sithean Mor. Pods of this layer continue for over 10 m at this horizon in the layered sequence. (Pen at the right of image gives scale). (c) Syn-magmatic disruption of partially layered (olivine and plagioclase-rich) cumulate at Achnaha (adapted from O'Driscoll, 2007). Camera lens cap in left centre of image is 5 cm in diameter. (d) Fine (centimetre) scale modal layering of plagioclase and pyroxene in the Druim Hain gabbros. Camera lens cap in centre of image is 5 cm in diameter. (e) Phase layering of magnetite (dark layers) and plagioclase-rich gabbro at Druim Hain (hammer at the centre of image for scale). (f) Large altered basalt dropstone down-warping magnetite and plagioclase-rich phase layering; the dropstone is ~4 m in length.

packages each ~3 m thick. Layering here is typically almost monomineralic, with layers of anorthosite or magnetite dominating (Fig. 2e). These packages, along with the layering and mineral lamination, undulate along

strike, suggesting a degree of syn-magmatic deformation. The eastern side of the intrusion (the top of the sequence or roof-zone) is characterized by xenoliths of varying composition and size (from centimetres to tens of metres

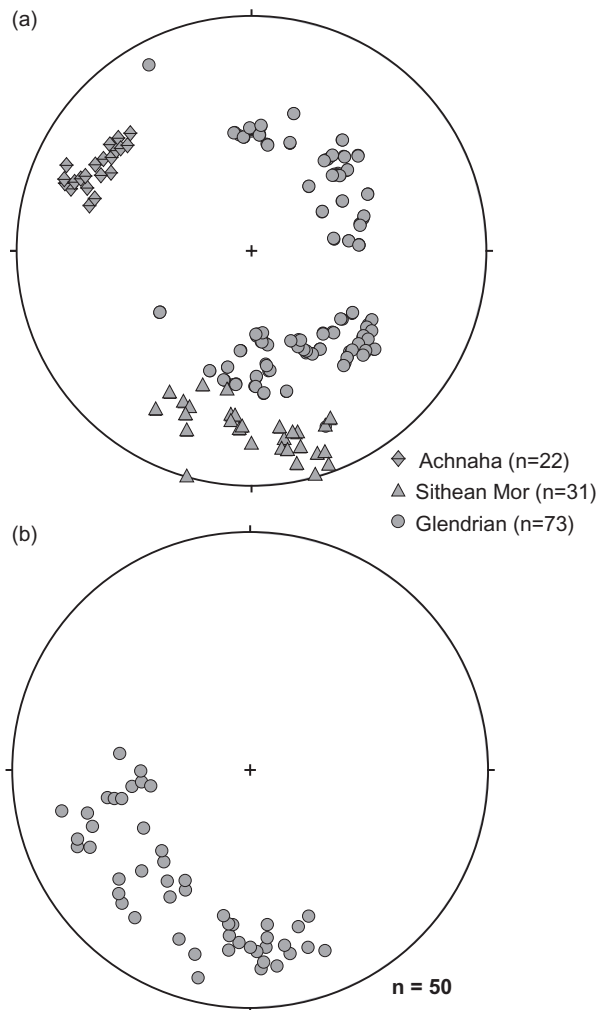


**Fig. 3.** Equal-area lower hemisphere stereographic projection of poles to mineral lamination data from all of (a) the Ardnamurchan laminated gabbros (adapted from O'Driscoll *et al.*, 2006) and (b) the Druim Hain layered gabbros. North is to the top in each diagram.

in diameter). These include fragments of Lewisian gneiss, fine-grained mafic xenoliths and greenish highly altered blocks of basalt or peridotite. Here, layering is poorly developed, and the rocks are highly altered and intruded by felsic and mafic pegmatites and dykes.

Mineral lamination (and layering) in the Druim Hain gabbros strikes parallel to the outer contacts of the intrusion and dips inward uniformly toward a focal point beneath the Meall Dearg granophyre of the Srath na Creitheach Centre (Fig. 3b), whose intrusive contacts bound the eastern side of the gabbros. A distinct steepening-inward trend is observed ( $\sim 30^\circ$  to  $\sim 70^\circ$ ) as this focal point is approached. With the exception of the ubiquitous mineral lamination, little evidence has been observed in the Druim Hain gabbros for small-scale structures associated with layering (such as slumping or trough layers). Toward the roof (east) of the intrusion, however,

sporadic fine-grained mafic blocks (dropstones) are sometimes observed deforming the layered sequence beneath them and in two cases are very large, measuring 4.5 m and 7 m in diameter (e.g. Fig. 2f). Graded bedding is observed at only one location; in an olivine-rich gabbro at the centre of the Druim Hain layered gabbro. This concurs with the assertion of Wager & Brown (1968) that 'sedimentary-type' structures are 'rare' throughout the Druim Hain layered sequence. There is thus a lack of direct field evidence for primary sedimentary processes in the development of layering at Druim Hain. However, the consistent steepening-inward (eastward) from  $\sim 30^\circ$  to  $\sim 70^\circ$  of layering and lamination planes may be due to large-scale central sagging of the layering, similar to that observed in the Rum Layered Suite (Emeleus *et al.*, 1996; O'Driscoll *et al.*, 2007b), the Ardnamurchan Great Eucrite (O'Driscoll *et al.*, 2006) (NW Scotland) and the Bushveld Complex of South Africa (Carr *et al.*, 1994). Whether this reflects central subsidence of the Cuillin Complex as a whole, or of a separate younger Druim Hain intrusion is, however, beyond the scope of this study.

## PETROGRAPHY

### Ardnamurchan laminated gabbros

The Ardnamurchan laminated gabbro samples are all similar in texture (including grain size) and mineralogy. Abundant subhedral (prismatic) plagioclase crystals (50–75 vol. %) form a cumulus framework that defines a lamination of variable strength in all samples (e.g. Fig. 4a). Plagioclase crystals are generally 'stubby' and in the size range 1–5 mm. Thin-sections cut parallel to the plane of mineral lamination show that the majority of crystals have (010) faces parallel or close to parallel to the plane. Plagioclase crystals are often zoned (Fig. 4b), although this feature is better observed on sections cut parallel to the lamination than perpendicular to it. No evidence for compaction (e.g. solid-state deformation of cumulate) is observed. Although the lamination is mainly defined by plagioclase, euhedral elongate prismatic clinopyroxene crystals (up to 5 mm in size) also occur parallel to the lamination. Clinopyroxene may also occur as anhedral (interstitial) clusters of crystals. Both reflected and transmitted light microscopy indicate that large (generally  $>150 \mu\text{m}$ ) magnetite crystals are a common, irregularly dispersed, constituent of the rock (10–15 vol. %). Magnetite varies in mode of occurrence from equant euhedral cumulus crystals to anhedral shapes; the latter frequently occur moulded onto cumulus plagioclase and clinopyroxene crystals (Fig. 4c). Minor orthopyroxene and olivine may be present, and aggregates of greenish-coloured amphibole and biotite sometimes occur closely associated with clinopyroxene.

Aligned plagioclase and clinopyroxene cumulus crystals in the laminated gabbros frequently lack well-defined

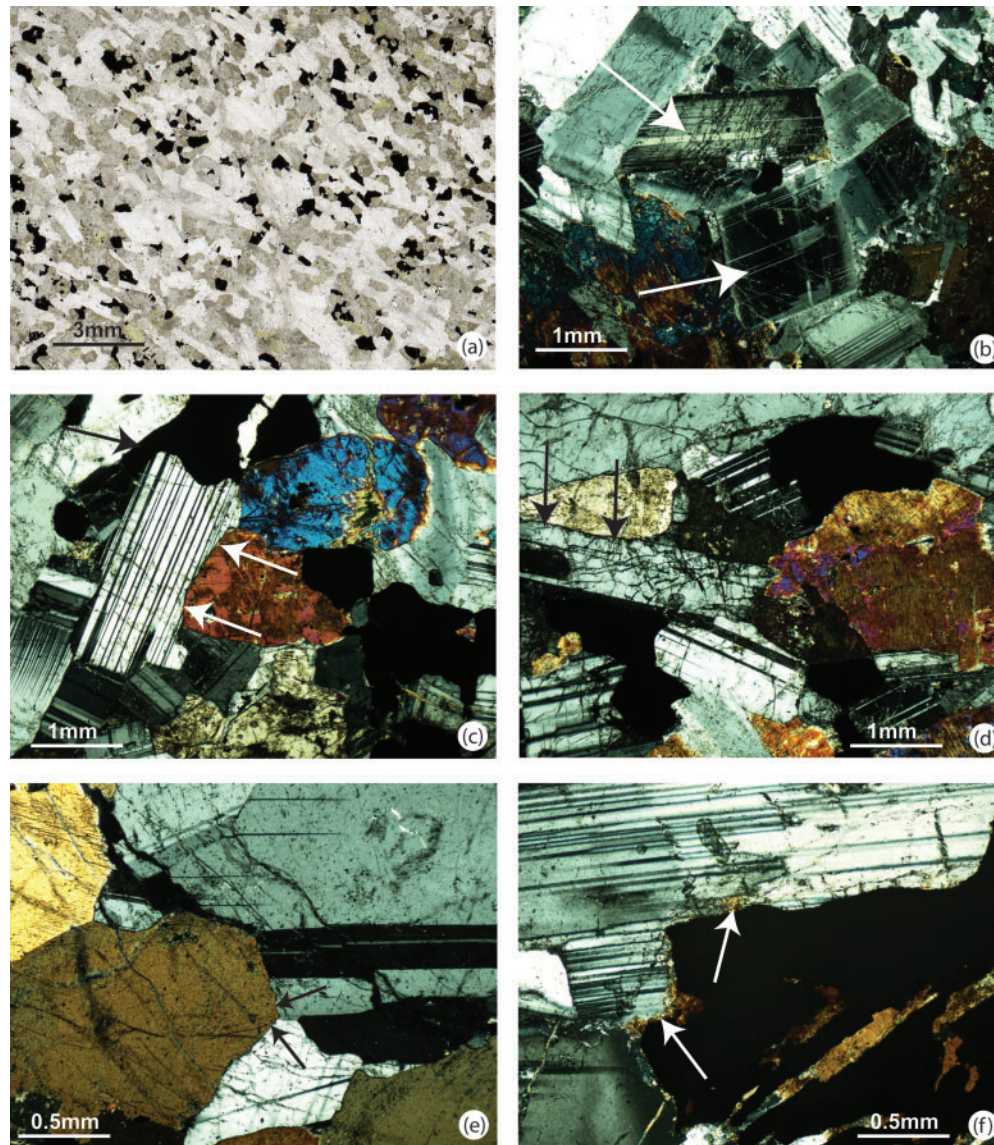


**Fig. 4.** (a) Typical sample of the Ardnamurchan laminated gabbro in plane-polarized light; thin-section cut normal to lamination, which runs NW–SE across the image. (b) Well-developed zoning in plagioclase crystals (highlighted) from the Sithean Mor laminated gabbro. (c) Intercumulus magnetite around plagioclase crystal (black arrow) and concave indented boundary of the same plagioclase crystal with clinopyroxene (white arrows). (d) Slightly concave upper boundary of plagioclase crystal with clinopyroxene (black arrows). (e) Typical plagioclase–plagioclase–clinopyroxene dihedral angle in the Glendrian laminated gabbro (black arrows). (f) Textural relationship between intercumulus magnetite and plagioclase; the presence of a thin impermanent rim of biotite around the plagioclase crystal should be noted (white arrows).

planar edges. This is because the interstitial pockets of anhedral clinopyroxene and magnetite, often intergrown with each other, have irregular and intricate crystal boundaries with the framework-forming plagioclase crystals, often appearing to grow into the latter in a manner resembling consertal texture. The effect of this is to cause concave indentations in the plagioclase crystals that form the cumulus framework and a deviation from a euhedral crystal shape (Fig. 4c and d). Observations on the degree of opening of median clinopyroxene–plagioclase–plagioclase dihedral

angles at triple grain junctions reveal that, in general, the majority of apparent dihedral angles are  $\geq 90^\circ$  (Fig. 4e). These are similar to baseline median dihedral angle values for olivine–plagioclase–clinopyroxene–spinel assemblages in the similarly sized Rum Eastern Layered Series (Holness, 2005), and somewhat less ( $\sim 10^\circ$ ) than baseline median values for the Lower Zone of the larger Skaergaard Complex (Holness *et al.*, 2007). A further petrographic feature of note is the manner which, in some interstitial areas, magnetite is separated from plagioclase and pyroxene

by thin rims of biotite (or another pleochroic micaceous alteration product) (Fig. 4f).

### Druim Hain layered gabbros

In contrast to the Ardnamurchan laminated gabbros, the Druim Hain layered gabbros vary considerably in texture, grain size and mineralogy, as a result of the well-developed outcrop-scale mineral layering they contain. In general, plagioclase and clinopyroxene prisms (up to 1 cm in length) form a cumulus framework that defines the mineral lamination in a manner similar to that of the Ardnamurchan rocks. However, in the Druim Hain samples, the mineral lamination may be carried predominantly by plagioclase (e.g. Samples 6, 8 and 23 of this study; Fig. 5), clinopyroxene (Samples 4 and 15 of this study, Fig. 6a), or both (Sample 18). Both minerals thus occur in varying amounts (together forming up to 75% by volume of the samples studied), sometimes contributing equally to the mineral lamination or sometimes such that one is almost negligible as a fabric-forming mineral.

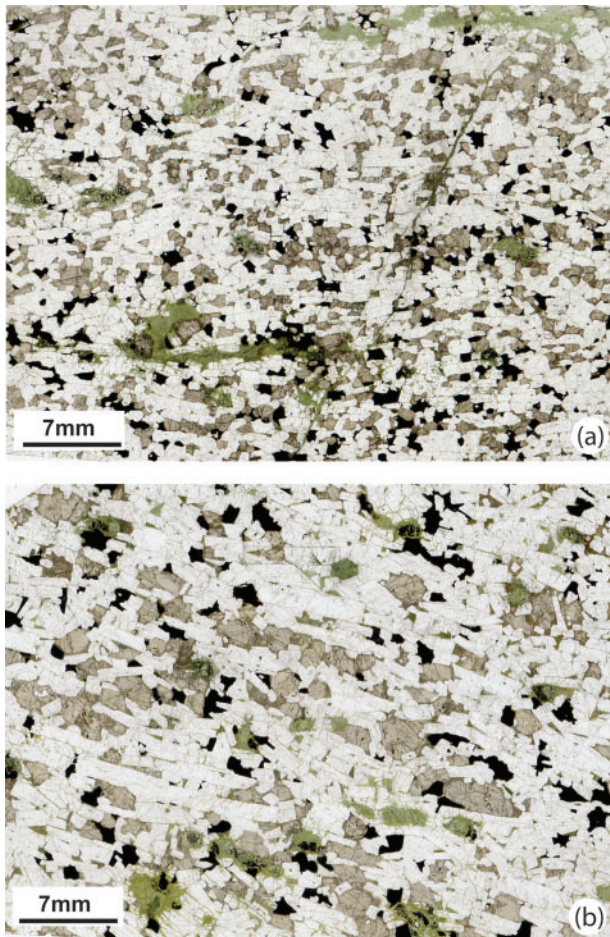


**Fig. 5.** (a) Plagioclase lamination at Druim Hain carried by short, 'stubby' crystals (Sample 8), and (b) by elongate, 'bladed' crystals (Sample 23).

The mineral lamination also varies in intensity. Although this may be partly attributed to some minerals (e.g. olivine) being less suited to carrying such a fabric than plagioclase, variation in the intensity of lamination is also observed where plagioclase or clinopyroxene alone are the volumetrically dominant phases, and appears to be related to grain size and aspect ratio of the fabric-forming mineral (see Fig. 5a and b). Clinopyroxene may also occur in interstitial pockets dispersed throughout the crystal framework. Several of the coarse-grained samples (e.g. 4 and 23) contain plagioclase and clinopyroxene crystals that display notable evidence of crystal-plastic strain (see Nicolas, 1992; McBirney & Nicolas, 1997), including deformation twinning and intra-crystal dislocation structures (Fig. 6b and c). Some plagioclase crystals in Sample 23 also exhibit well-developed strain shadows. It is noteworthy that samples with a smaller grain size have not developed these crystal-plastic strain features to the same extent. Where present, zoning of plagioclase is usually subtle and poorly developed. As mentioned above, minor (<5 vol. %) amounts of cumulus olivine are observed, and some alteration of clinopyroxene to greenish amphibole occurs. Reflected light microscopy indicates that the principal oxide mineral phase present in the Druim Hain rocks is magnetite. In general, magnetite occurs as irregularly spaced equant crystals making up ~5–10 vol. % of the rock. However, several samples contain up to 30 vol. % magnetite, as anhedral crystals in orthocumulates in which plagioclase and clinopyroxene are also present (Figs. 6a and f). These magnetite textures resemble orthocumulates from the Lower Zone of the Skaergaard intrusion, in which magnetite has been shown to be a cumulus phase (M. B. Holness, personal communication, 2008).

A notable feature of all of the Druim Hain rocks is the preservation of the planar edges of the framework-forming minerals in most samples, particularly those of plagioclase (Figs 5b and 6d). An important feature of this texture is that the intercumulus minerals occur in clean, well-defined interstitial pockets in the cumulus framework. Optical examination reveals that this feature is accompanied by clinopyroxene–plagioclase–plagioclase apparent dihedral angles at triple grain junctions that average out at significantly lower values than those for the Ardnamurchan samples (i.e. ~40–70°; Fig. 6e). The samples with large quantities of magnetite (e.g. Sample 15) often contain magnetite crystals that enclose clinopyroxene and/or plagioclase crystals that are well-rounded and show constant mean curvature of grain boundaries (Fig. 6f). These textures indicate melt-present textural equilibrium (e.g. Holness *et al.*, 2005), where magnetite has pseudomorphed the interstitial melt. In samples with abundant magnetite, some overgrowth on cumulus magnetite crystals has occurred, so that indentations and irregular grain boundaries are observed between magnetite and/or plagioclase and clinopyroxene

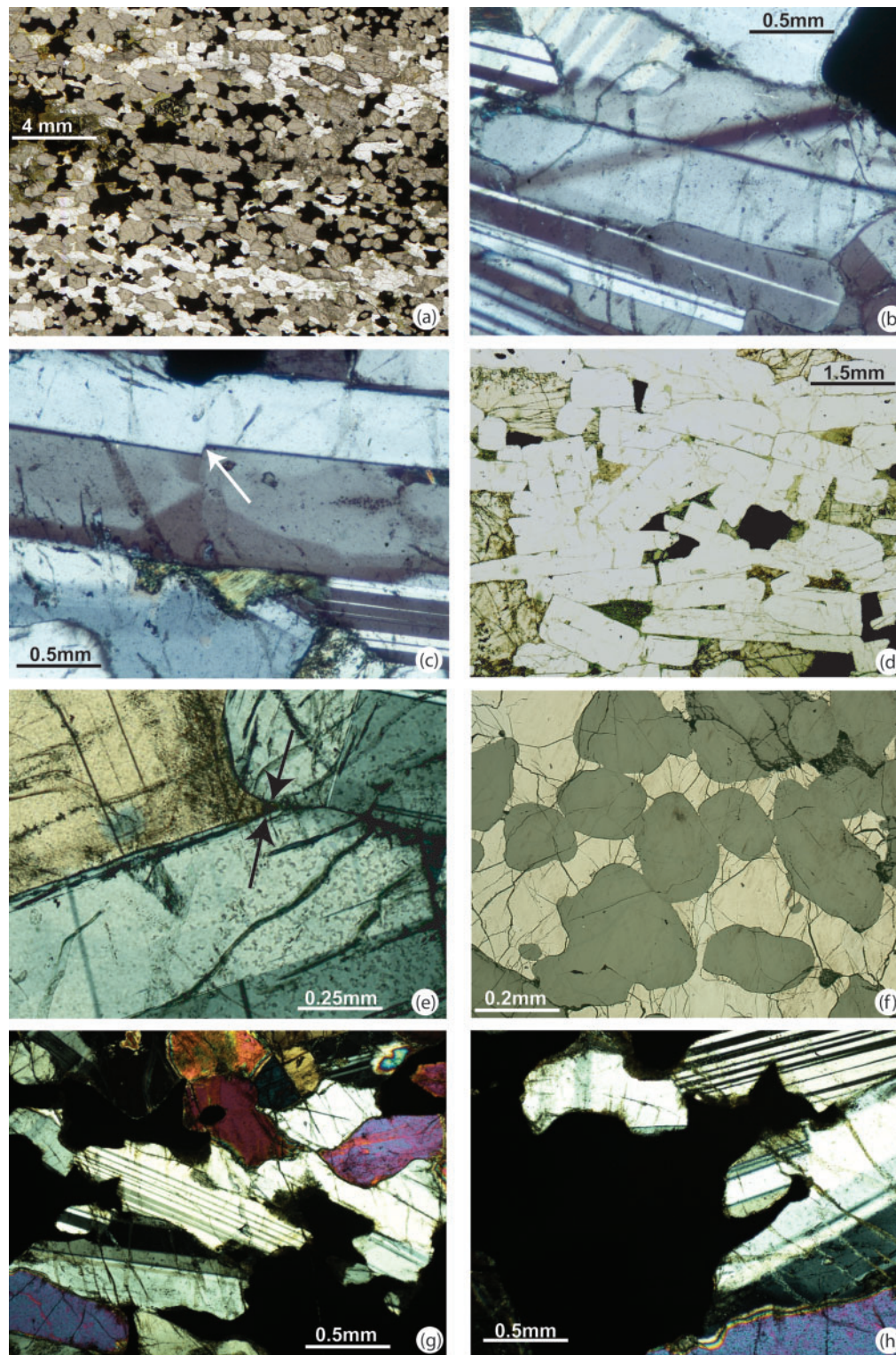


**Fig. 6.** (a) Thin-section image of Sample 15, in which clinopyroxene is the dominant fabric-forming mineral. The presence of intercumulus magnetite and thin plagioclase-rich zones should be noted. (b) Deformation twin superimposed on magmatic twinning in plagioclase. (c) Minor dislocation (arrowed) in plagioclase magmatic twin plane. Both (b) and (c) are from Sample 23 and are cut perpendicular to mineral lamination. (d) Plane-polarized image of Sample 23, illustrating typical clean straight plagioclase crystal boundaries. (e) Typical plagioclase–plagioclase–clinopyroxene dihedral angles in the Druim Hain layered gabbro (black arrows). (f) Reflected light image of Druim Hain cumulate showing relationships between magnetite (bright areas) and rounded pyroxene crystals. The low clinopyroxene–clinopyroxene–magnetite dihedral angles, suggestive of melt-present equilibrium, should be noted. (g, h) Textural readjustment, leading to overgrowth on cumulus magnetite crystals, has resulted in complex indentations in plagioclase grains in Sample 15. (Note rounding of grains and truncation of plagioclase twins.)

crystals (Fig. 6g and h). These indentations and embayments crosscut or truncate solid-state deformation textural features.

## PETROFABRIC ANALYSIS

### Anisotropy of magnetic susceptibility

Anisotropy of magnetic susceptibility (AMS) is controlled mainly by the preferred orientation of magnetic grains in a rock, principally the ferromagnetic (e.g. magnetite) and paramagnetic mineral phases (e.g. olivine, hornblende). In this study, samples, oriented by compass, were collected and from each block 10–16 (typically 12) specimens of  $\sim 11 \text{ cm}^3$  were drilled in the laboratory (see Owens, 1994). These were measured on an AGICO KLY-3S Kappabridge (an induction bridge that operates at a magnetic field of 377 mT and a frequency of 875 Hz) at the University of Birmingham, UK. Susceptibility differences were measured in three orthogonal planes and combined with a measurement of one axial susceptibility to define the susceptibility tensor. Assuming that the specimens from a block represent a homogeneous multinormal population, results are reported for block averages of specimen AMS tensors, normalized by specimen mean susceptibility. Within-block variability is characterized through calculation of the 95% confidence limits on direction and magnitude parameters using a tensor-averaging process (Jelínek, 1978; Owens, 2000a).

The magnetic susceptibility tensor, which may be pictured as an ellipsoid, comprises the three principal susceptibility magnitudes ( $K_1 \geq K_2 \geq K_3$ ), and a corresponding set of three orthogonal principal axis directions. The magnitude parameters are usually reported in terms of 'size', 'shape' and 'strength' (or ellipticity) of the ellipsoid. The parameters adopted in this study are (see Owens, 1974, 2000b)

$$\begin{aligned} K_{\text{mean}} &= (K_1 + K_2 + K_3)/3 \\ L &= (K_1 - K_2)/K_{\text{mean}} \\ F &= (K_2 - K_3)/K_{\text{mean}} \\ H &= L + F = (K_1 - K_3)/K_{\text{mean}} \\ m &= L/F, \mu = \tan^{-1} m \end{aligned}$$

where a plot of L (the magnetic lineation) over F (the magnetic foliation) provides a graphical representation of the shape and strength of the ellipsoid. H (quoted as a percentage) defines the strength of the magnetic fabric (see also Liss *et al.*, 2002; O'Driscoll *et al.*, 2006; Stevenson *et al.*, 2007a). The shape of the ellipsoid is described by  $\mu$ . The AMS fabrics in all of the samples described in this study are carried by magnetite (see below), meaning that the magnetic fabrics reflect a bulk magnetite grain-shape fabric. A more comprehensive introduction to the AMS technique, with an explanation of this and other details of AMS theory, is provided in the Appendix.

At Ardnamurchan, four oriented blocks were collected from the Achnaha area, eight from the Sithean Mor area and 11 from the Glendrian area (Fig. 7). Several sites were double and triple sampled, to test for within-site variation. From Skye, 23 oriented block samples were collected from the well-laminated upper portion of the Druim Hain gabbros (the lower poorly layered 100–200 m of the sequence were not considered for the purposes of this study; Fig. 8). Double sampling of (two) sites on Druim Hain was carried out to test for within-site variation.

### AMS results

#### *Ardnamurchan laminated gabbros*

All of the AMS data for the Ardnamurchan samples are summarized in Fig. 7 and Table 1. The Glendrian laminated gabbro exhibits the highest values of  $K_{\text{mean}}$  with an average of  $2.3 \times 10^{-1}$  (SI units); average  $K_{\text{mean}}$  values for the Achnaha and Sithean Mor areas are  $9.7 \times 10^{-3}$  and  $1.4 \times 10^{-1}$ , respectively. In magnetite bearing rocks, magnetic susceptibility is usually a function of the volume of magnetite in a sample (e.g. Balsley & Buddington, 1958), and the data presented here are consistent with average volume concentrations of magnetite of  $\sim 9\%$ , supporting the conclusions drawn from the reflected light microscopy. Anisotropy strength (H) across the three areas is usually in the range 8 to 15% and the shape of the anisotropy is variable (Fig. 9a). There is a close correspondence between the orientation of magmatic foliations and mineral lamination measured in the field in all three areas (Fig. 9b). Although exceptions exist (e.g. in the Sithean Mor gabbro), magnetic lineations are usually disposed downdip on magnetic foliations and thus plunge confocally.

#### *Druim Hain layered gabbros*

All of the Druim Hain AMS data are summarized in Fig. 8 and Table 2.  $K_{\text{mean}}$  values for the Druim Hain layered Gabbros are between  $6 \times 10^{-3}$  and  $166 \times 10^{-3}$ , again consistent with abundant magnetite (in average volume concentrations of 6–7%). H values are distributed, seemingly normally, between 7 and 25%. The shape parameters, unlike those for the Ardnamurchan samples, show a propensity to oblateness in the more anisotropic samples (Fig. 9a). Again, there is a close agreement between the mineral lamination and layering measured in the field and the magnetic foliation (with the exception of Sample 11), but in this case, the magnetic lineations are not consistently oriented downdip (Figs 8 and 9c), and generally display very inconsistent orientations.

### Intercept counting technique

It has been shown above that the AMS foliation in almost all samples closely parallels the mineral lamination observed in the field (Fig. 9b and c). However, verification that the measured AMS lineations reflect the petrofabric of the samples is required. To investigate the presence

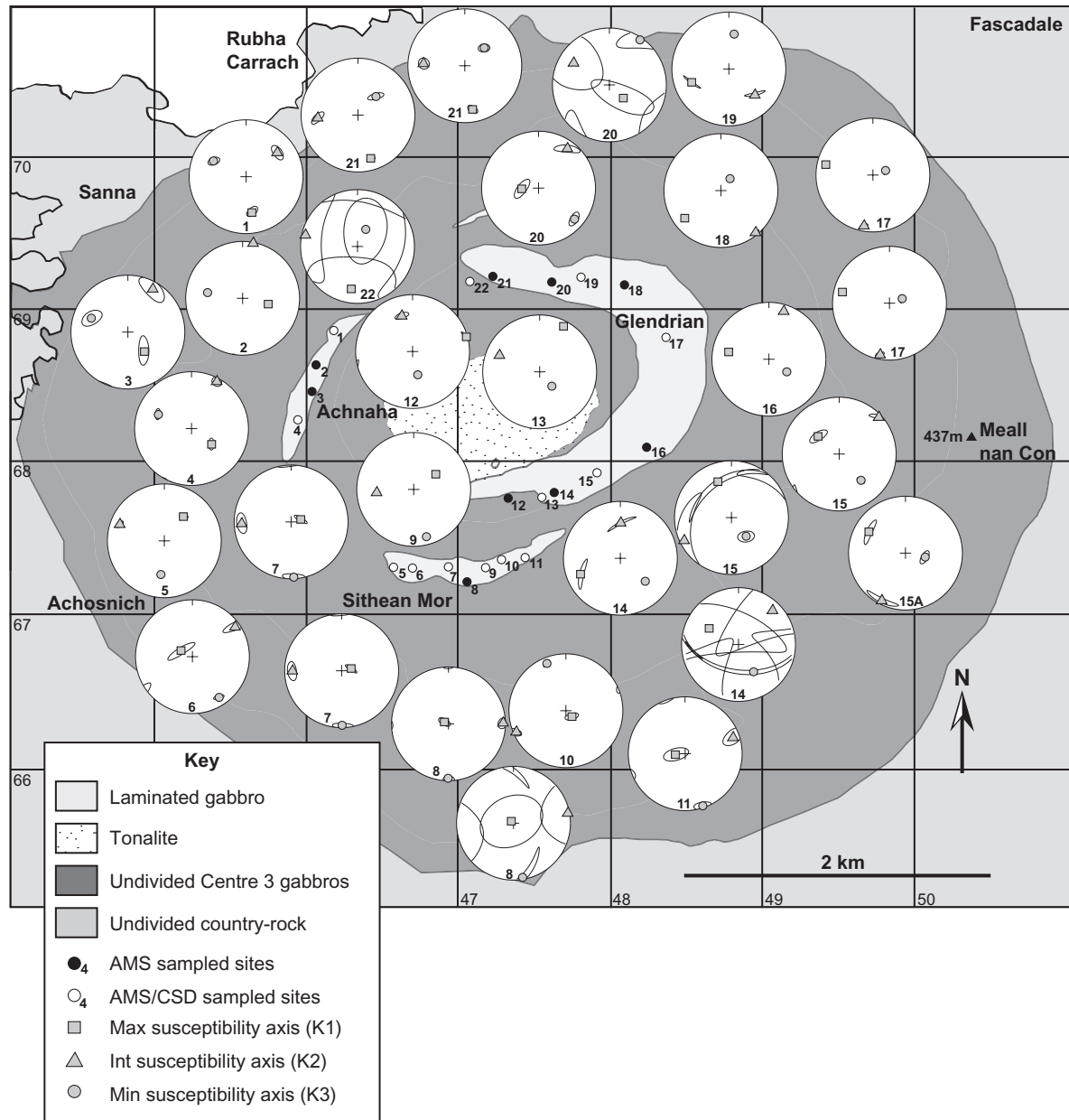


**Fig. 7.** Ardnamurchan laminated gabbro AMS data.  $K_1$ ,  $K_2$  and  $K_3$  are plotted on equal-area stereographs for all samples.

of linear arrangements of silicate crystals on the mineral lamination planes, the intercept counting method of Launeau & Robin (1996) was applied to thin-sections from a subset of the oriented AMS blocks, cut parallel to the mineral lamination (and hence the AMS foliation), and with one edge parallel to the direction of dip of the lamination plane. Multispectral analysis of scanned images of thin-sections was employed to characterize the colour of the different mineral phases and to classify each pixel in the image. For the Ardnamurchan samples, plagioclase and magnetite were tested for Samples 4, 5,

6, 15 and 19. For the Druim Hain samples, plagioclase and magnetite were examined in Samples 18 and 23, and clinopyroxene and magnetite were examined in Samples 15 and 18. The possible error in orientation of the thin-sections, as a result of cumulative errors in cutting and preparation, is estimated at  $\leq 5^\circ$ .

The intercept counting technique analyses a digitized sample area along a set of parallel lines (see Launeau & Robin, 1996). The number of intersections between the boundaries of the mineral phases and the analysis lines are counted in each direction, and the results displayed

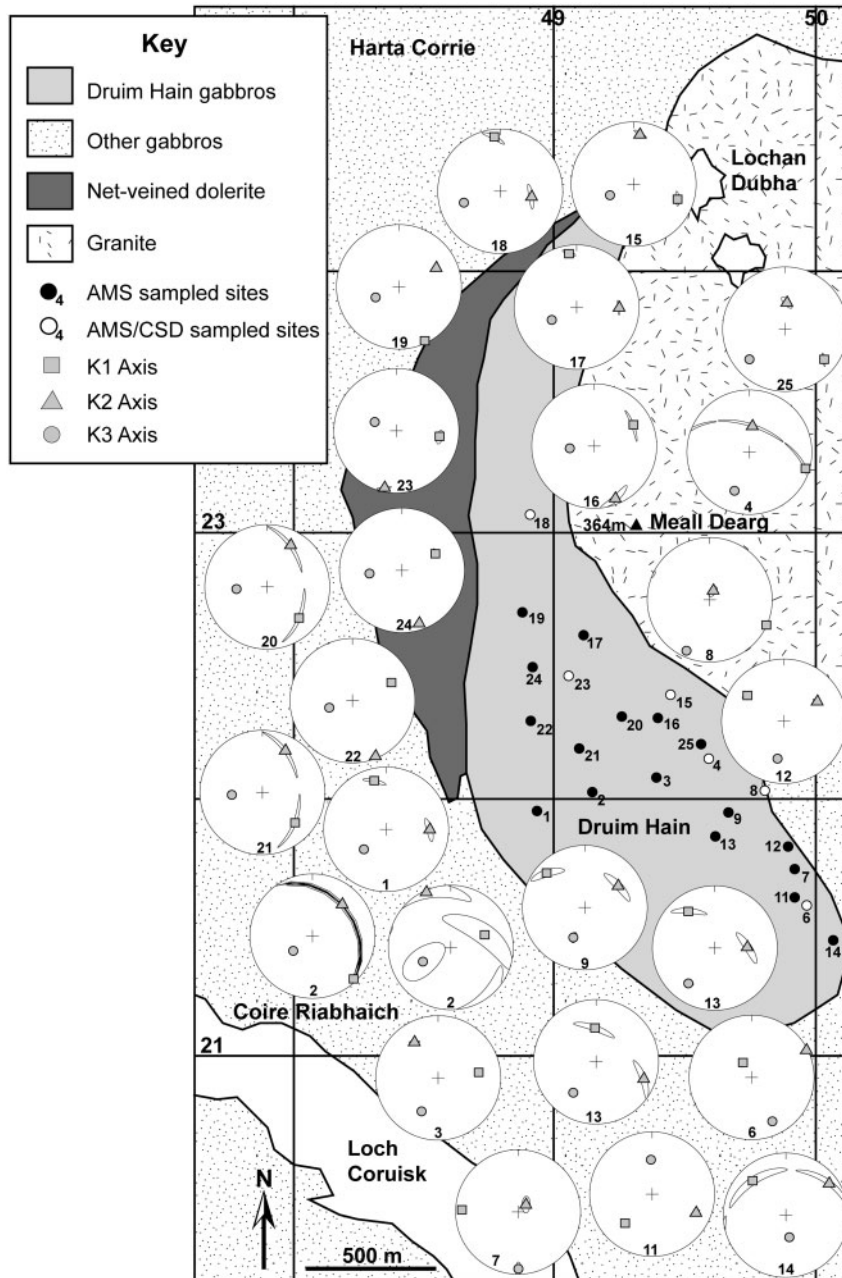


**Fig. 8.** Drum Hain layered gabbro AMS data.  $K_1$ ,  $K_2$  and  $K_3$  are plotted on equal-area stereographs for all samples.

as a ‘rose of intercept counts, which is a polar histogram of the number of counts of a given phase versus the angle of analysis’ (Launeau & Cruden, 1998). The minimum count direction corresponds to the elongation of the phase boundaries. The intercept method examines only crystal boundaries, thus it is not necessary for single crystals to be separated from each other for the 2D shape preferred orientation (SPO) of a given mineral phase in a sample to be calculated. A rose of boundary directions may also be extracted from the intercept data, and can be used

to investigate the presence of sub-fabrics within the crystal population with orientations oblique to the long axis of the bulk fabric. Here we follow the system of Launeau & Cruden (1998):  $A$  and  $B$  are the maximum and minimum directions of roses of mean intercept lengths;  $S_R$  describes the shape ratio of the lineation measured. The angle  $\alpha$  is the angle between the mineral lineation (as calculated by the intercept method) and the direction of dip of the mineral lamination plane, and thus describes the orientation of the lineation.

Table 1: Ardnamurchan AMS data

Sample no.	$K_{\text{mean}}$	$K_1$	Dec.	Inc.	$K_2$	Dec.	Inc.	$K_3$	Dec.	Inc.	L	F	H	$\mu$
<i>Achnaha</i>														
1	4.52	1.04	170	37.8	1.01	52.5	30.7	0.95	115.8	-37.1	3.64	5.11	8.75	35.5
2	12.09	1.05	102.7	52.5	1.01	10.5	1.7	0.94	99.2	-37.4	4.07	6.65	10.72	31.5
3	9.9	1.04	139.5	54.5	1.02	29.9	13.4	0.95	111.3	-32.1	2.38	6.97	9.35	18.8
4	12.4	1.05	127.9	53.5	1.01	28.3	7	0.95	113.2	-35.6	3.79	6.14	9.93	31.7
<i>Sithean Mor</i>														
5	18.06	1.04	218.5	-44.5	1.01	110.5	-17.5	0.95	5	-40.3	3.63	5.22	8.86	34.8
6	101.7	1.04	116.2	-71.8	1.01	54.5	8.9	0.95	327	-15.8	3.55	5.27	8.82	34
7A	92.89	1.05	258.9	-76.1	1	89.5	-13.6	0.96	358.9	-2.4	5.06	3.72	8.78	53.7
7B	93.7	1.05	255.2	-75.7	1	88.4	-13.9	0.96	357.6	-3.1	5.1	3.61	8.71	54.8
8A	160.84	1.06	114.7	-83.7	1.01	89.5	5.7	0.93	359.7	-2.7	5.47	8.21	13.68	33.7
8B	150.73	1.06	132.3	-85.7	1	79.8	2.6	0.94	350	-3.4	5.57	6.54	12.11	40.4
9	143.01	1.04	235.7	-51.1	1.03	85.1	-35.1	0.93	344.6	-14.6	1.58	10.17	11.75	8.8
10	249.73	1.06	314.9	-78.2	1.03	66.7	-4.4	0.92	337.6	10.9	3.44	11.04	14.47	17.3
11	208.64	1.05	86.3	-76.8	1.01	71	12.8	0.94	341.7	-3.4	3.99	7.28	11.27	28.7
<i>Glendrian</i>														
12	252.28	1.08	254.9	-2.2	1.01	343.4	34.5	0.91	168.1	55.5	7.15	9.86	17.01	35.9
13	238.16	1.05	26.7	10.6	1.01	111.9	-24.3	0.94	138.5	63.2	4.58	6.98	11.56	33.3
14A	239.63	1.05	67.9	-27.5	1.04	1.4	37.4	0.91	311.8	-40.3	1.57	12.6	14.17	7.1
14B	221.73	1.07	118.7	-41.7	0.99	44.4	16.9	0.94	331.1	-43.4	8.61	4.51	13.11	62.4
15A	245.08	1.04	339.8	33.5	1.02	64.4	-8.2	0.94	142.4	55.3	1.93	8.06	9.98	13.5
15B	251.36	1.05	300.6	27.1	1.02	26.7	-7.6	0.93	102.4	61.7	2.96	9.72	12.68	16.9
15C	243.67	1.04	130.5	-50	1.02	46.7	5.1	0.94	320.9	-39.6	2.1	7.53	9.64	15.6
15D	224.4	1.05	279.6	33.6	1.02	14.7	7.6	0.93	115.8	55.3	3.24	8.5	11.73	20.8
16	227.04	1.05	280.1	29	1.02	16.7	11.8	0.93	126.5	58.2	3.73	8.24	11.97	24.4
17A	217.78	1.05	282.9	16.1	1	10.1	-9.6	0.95	70.5	71.1	4.8	4.85	9.64	44.7
17B	217.44	1.05	283.3	16	1	10.5	-9.4	0.95	71.2	71.3	4.68	4.94	9.63	43.4
18	207.49	1.04	52.8	-21.2	1.02	140.8	5	0.95	38.1	68.1	2.28	6.98	9.26	18.1
19	210.91	1.03	69.9	-31	1.02	133.7	36.4	0.95	8.2	38.3	1.25	7.61	8.86	9.4
20A	214.76	1.01	313.8	-62.4	1	121.7	-27	0.99	34.3	5	1.06	1.52	2.58	34.8
20B	276.42	1.05	267.9	66	1.01	35.9	15.3	0.94	131	18	4.09	7.58	11.67	28.4
21A	261.92	1.07	349.9	-22.8	0.98	93.1	-28.6	0.95	47.3	52	8.36	3.62	11.98	66.6
21B	239.69	1.04	332	-14.3	1.02	65.7	-14.2	0.94	18.8	69.6				
21C	257.75	1.07	343.5	-21	0.99	86.1	-29.5	0.94	43.5	52.4	8.18	4.26	12.44	62.5
22A	119.55	1.02	8.7	-25.8	1	102	-6.8	0.98	25.6	63.2	1.75	2.22	3.97	38.2
22B	271.2	1.05	60.5	9.6	1.01	316.9	54.2	0.94	337.1	-34.1				

Dec. (declination) and Inc. (inclination) of susceptibility axes.  $K_{\text{mean}}$  is in  $10^{-3}$  SI units. (See text for parameter definitions.)

## Intercept results

### *Ardnamurchan laminated gabbros*

Excellent agreement is observed between the lineation directions exhibited by magnetite and plagioclase; the maximum difference between them is  $11^\circ$  (Fig. 10). There is a suggestion in some samples that a second subordinate lineation (consistent for both plagioclase and magnetite)

may be present (e.g. Sample 4), but there is insufficient evidence in the dataset to discuss this notion in further detail. It is notable also that almost all samples have lineations that are oriented approximately downdip on lamination planes, in good agreement with the AMS data (compare Fig. 10 with the AMS lineations in Fig. 7). Lineation orientations are the focus of this study, and it is

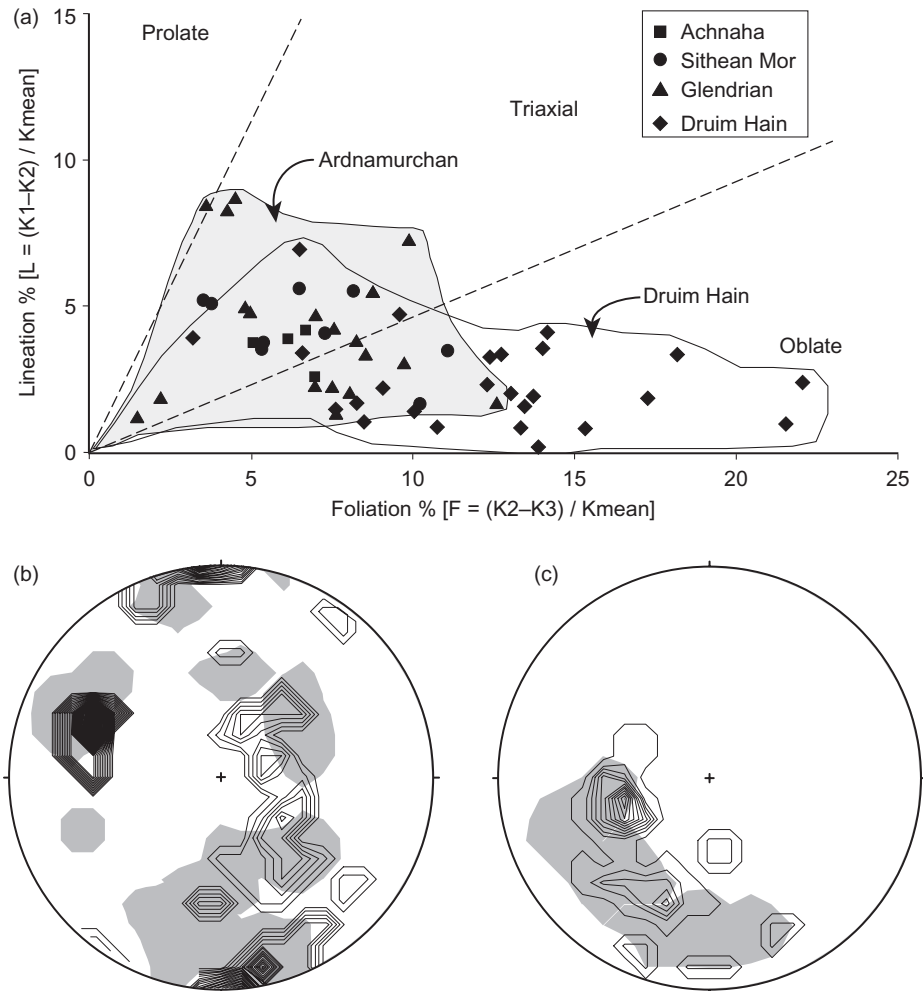


**Fig. 9.** (a) Plot of magnetic lineation against magnetic foliation for the Ardnamurchan and Druim Hain samples. The data fields for both sample localities are highlighted. (b, c) The poles to  $K_3$  data are contoured along with the field data from each locality (the latter is shown here in the grey shading), for the purposes of comparing both fabric datasets for the Ardnamurchan laminated gabbros and the Druim Hain layered gabbros, respectively.

beyond our scope to deal with the fabric shapes provided by the intercept method, principally as 3D ellipsoid data have not been calculated for our samples. However, it is informative to briefly compare the values of  $S_R$  returned by the intercept method with the values of  $L$  calculated from the AMS tensor (Table 1). The samples with a relatively strong plagioclase lineation as suggested by the intercept data (Fig. 10, higher values of  $S_R$ ) correspond to samples with high values of  $L$ . The one exception to this is the low value of  $S_R$  for magnetite in Sample 6.

#### *Druim Hain layered gabbros*

Sample 18 of the Druim Hain set shows a good agreement in lineation orientation between plagioclase and clinopyroxene. The magnetite lineation here deviates from this orientation by  $\sim 20^\circ$ , although it should be noted that

it corresponds to the AMS lineation orientation for this sample better than the plagioclase and clinopyroxene lineations do (see Fig. 11). However, for Samples 15 and 23, the magnetite lineation deviates from the clinopyroxene and plagioclase lineation directions significantly (by up to  $42^\circ$ ), and does not show convincing agreement with the AMS data (Fig. 8). No overall consistency is observed in lineation orientations, with Sample 18 having lineations oriented approximately parallel to the direction of strike of the lamination, and Samples 4 and 23 trending obliquely. Values of  $S_R$  show no apparent correlation with values of  $L$  from the AMS dataset (Fig. 11). The lack of consistency between AMS and intercept datasets might be due to the fact that the AMS technique is more sensitive than the intercept method; in two samples, 18 and 23, only very small amounts of magnetite are present ( $<3$  vol. %).

Table 2: *Druim Hain AMS data*

Sample no.	$K_{\text{mean}}$	$K_1$	Dec.	Inc.	$K_2$	Dec.	Inc.	$K_3$	Dec.	Inc.	L	F	H	$\mu$
S1	6.01	1.04	346.8	21.6	1.02	90.7	31.3	0.94	228.1	50.5	1.23	8.4	9.62	8.3
S2A	51.78	1.05	316.3	-4.3	1.05	43.7	31.5	0.91	233.3	58.2	0.13	13.92	14.05	0.5
S2B	65.08	1.04	248.6	-41.6	1.02	336.3	2.6	0.95	243.4	48.3	1.64	7.48	9.12	12.3
S3	137.97	1.07	82.2	35	1.03	326.9	31.4	0.89	27	-39.2	3.8	13.98	17.79	15.2
S4	25.29	1.08	106.5	7.2	1.07	6.3	54.6	0.85	21.4	-34.5	1.13	21.64	22.77	3
S6	148.28	1.06	148.4	-67.4	1.02	63.9	2.3	0.92	334.8	-22.4	4.93	9.48	14.41	27.5
S7	84	1.05	91.7	-10.2	1.01	47.3	75.9	0.95	360	-9.7	3.59	6.42	10.02	29.2
S8	146.02	1.04	114.1	0.4	1	22.1	78.7	0.97	24.1	-11.3	4.06	2.96	7.02	53.8
S9	6.59	1.07	312.5	19.2	1.03	57.2	36.1	0.9	200.2	47.6	3.51	12.6	16.11	15.6
S11	166.04	1.06	43.1	-36.4	1.04	113.5	24.4	0.9	357.8	43.7	2.02	13.64	15.66	8.4
S12	73.89	1.06	124.3	-28.4	1.03	59.6	38.2	0.91	8.7	-38.7	3.44	12.41	15.85	15.5
S13A	44.88	1.08	177.5	-44.9	1.05	109.8	20.9	0.87	37	-37.8	3.52	18.21	21.73	10.9
S13B	99.78	1.06	145.1	-28.1	1.04	88.8	46.1	0.91	36.7	-30.6	2.18	13.12	15.3	9.4
S14	18.09	1.05	316.9	24.7	1.04	53.6	14.3	0.91	170.8	60.9	0.99	13.33	14.32	4.2
S15	51.13	1.07	288.3	-27	1.05	7.8	19.6	0.88	246.4	55.6	2.01	17.26	19.27	6.6
S16	104.61	1.06	241.7	-30.6	1.04	337.8	-10.3	0.9	264.3	57.4	1.87	13.5	15.38	7.9
S17	12.19	1.04	352.2	12.8	1.03	90.7	33.1	0.93	244	53.9	1.56	9.98	11.54	8.9
S18	64.09	1.04	173.4	-13.9	1.02	99.7	48.5	0.94	72.2	-38.1	1.85	8.11	9.96	12.9
S19	59.7	1.04	254.5	-40.2	1.03	345.9	-1.7	0.93	257.9	49.8	1.01	10.61	11.62	5.4
S20	127.47	1.07	334.6	-1.7	1	63.4	34.4	0.93	247.1	55.6	7.13	6.36	13.49	48.3
S21	72.6	1.06	314	-29.5	1.05	28.7	25	0.9	265.6	49.5	0.94	15.29	16.23	3.5
S22	51.04	1.05	245.5	-31.7	1.02	337.4	-3.2	0.93	252.6	58.1	2.33	9.01	11.34	14.5
S23	32.29	1.09	278.4	-30.3	1.07	12	-6.2	0.84	292.3	58.9	2.59	22.17	24.76	6.7
S24	76.54	1.06	242.1	-40.5	1.03	342.1	-11.4	0.91	264.7	47.2	2.48	12.28	14.76	11.4
S25	94.03	1.08	128.4	21.8	1.03	3.9	54.7	0.89	49.7	-26.3	4.29	14.17	18.46	16.8

Dec. (declination) and Inc. (inclination) of susceptibility axes.  $K_{\text{mean}}$  is in  $10^{-3}$  SI units. (See text for parameter definitions.)

## CRYSTAL SIZE DISTRIBUTION ANALYSIS

Crystal size distribution (CSD) analysis provides a quantitative measure of the number of crystals of a mineral per unit volume within a series of defined size intervals. Crystal size in igneous rocks carries information on growth rate and nucleation, and thus CSDs have been used as a method of determining some of the crystallization kinetics of magmatic systems independent of experimental approaches and thermodynamic or kinetic models (e.g. Cashman & Marsh, 1988; Resmini & Marsh, 1995; Marsh, 1998; Higgins, 2002*b*; Boorman *et al.*, 2004). CSDs are usually plotted as population density (logarithmic number of crystals per unit volume) against crystal size (maximum length). An open-system (steady-state) model and a closed-system (batch) model are two end-member models suggested for igneous rocks from CSD studies (Marsh, 1988, 1998). It has been argued that simple crystallization (according to either model) exclusively leads

to a straight, or log-linear CSD plot representing (kinetic) textures solely developed through nucleation and growth (Higgins, 2006*a*). Kinking or curvature in the CSD plot profile has been attributed to many different processes (Higgins, 2006*b*); examples being crystal accumulation and removal (Marsh, 1998), compaction (Boorman *et al.*, 2004), mixing of crystal populations (Higgins, 2006*b*; Jerram *et al.*, 2003; Turner *et al.*, 2003) and post-nucleation crystal modification caused by annealing or Ostwald ripening.

Previous CSD studies on foliated cumulates have shown that primary magmatic textures may be modified by varying amounts as a result of coarsening and recrystallization in the crystal mush. The study of Boorman *et al.* (2004) on plagioclase and orthopyroxene cumulates of the Jagdlust Lower-Critical Zone section of the Bushveld intrusion argued that foliated cumulates formed largely as a result of compaction-driven recrystallization, a process that also involved an increase in crystal aspect ratio and fabric intensity. Higgins (2002*a*) did not observe evidence

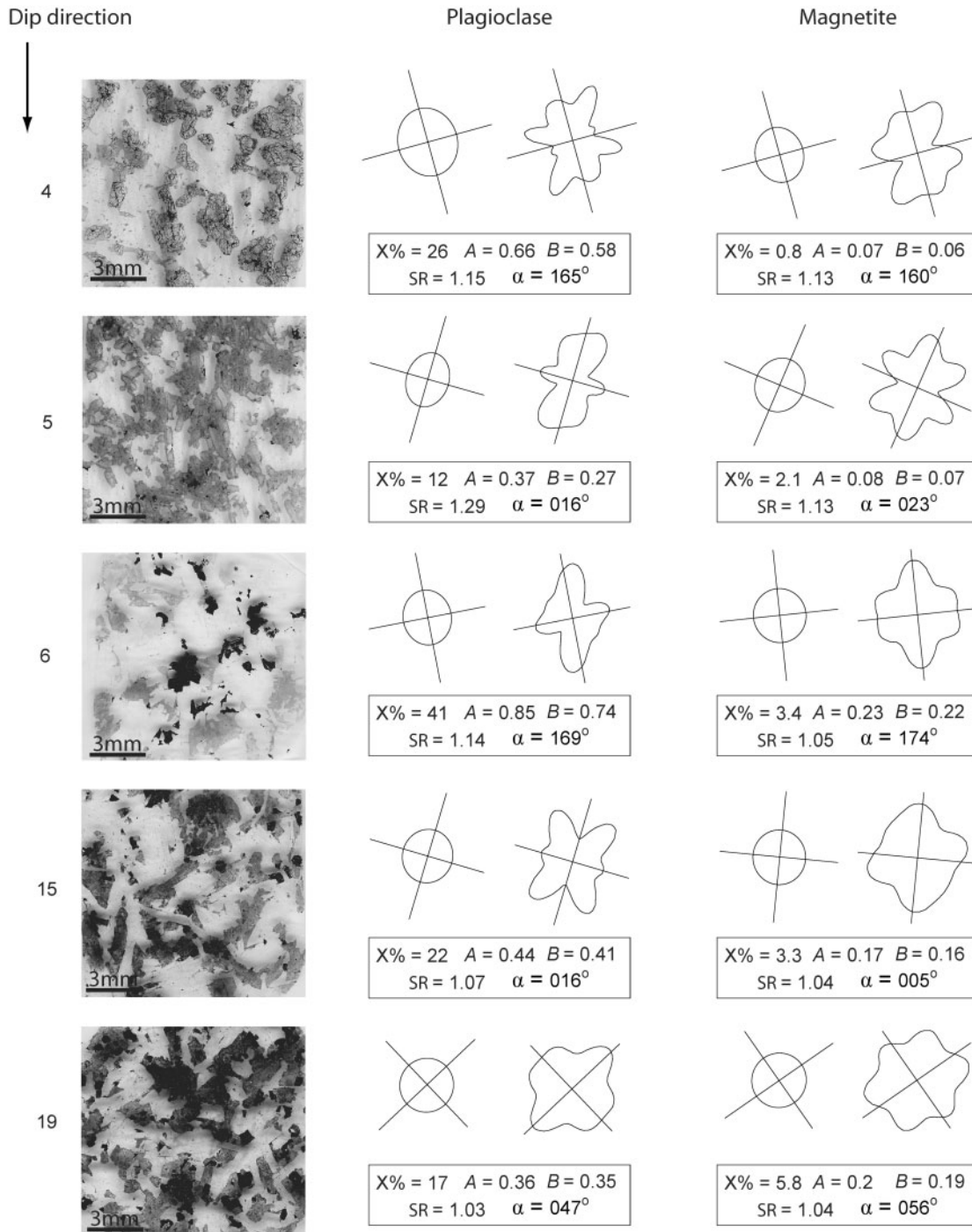


**Fig. 10.** Intercept petrofabric data for selected samples from the Ardnamurchan laminated gabbros (see text for details). Oriented sample numbers are given and the direction of dip is arrowed.

for compaction of plagioclase in the Kigaplait intrusion, Labrador, although he also suggested that simple recrystallization in the crystal mush (without crystal shape change) had occurred. Both of the latter studies suggested that significant recrystallization and modification of the crystal

mush requires the presence of a liquid, an observation that is discussed in more detail for this study below. We use CSD plot shape, specifically the magnitude of deviation from a log-linear profile for each of the sample localities, to gain insights into the textural history of the

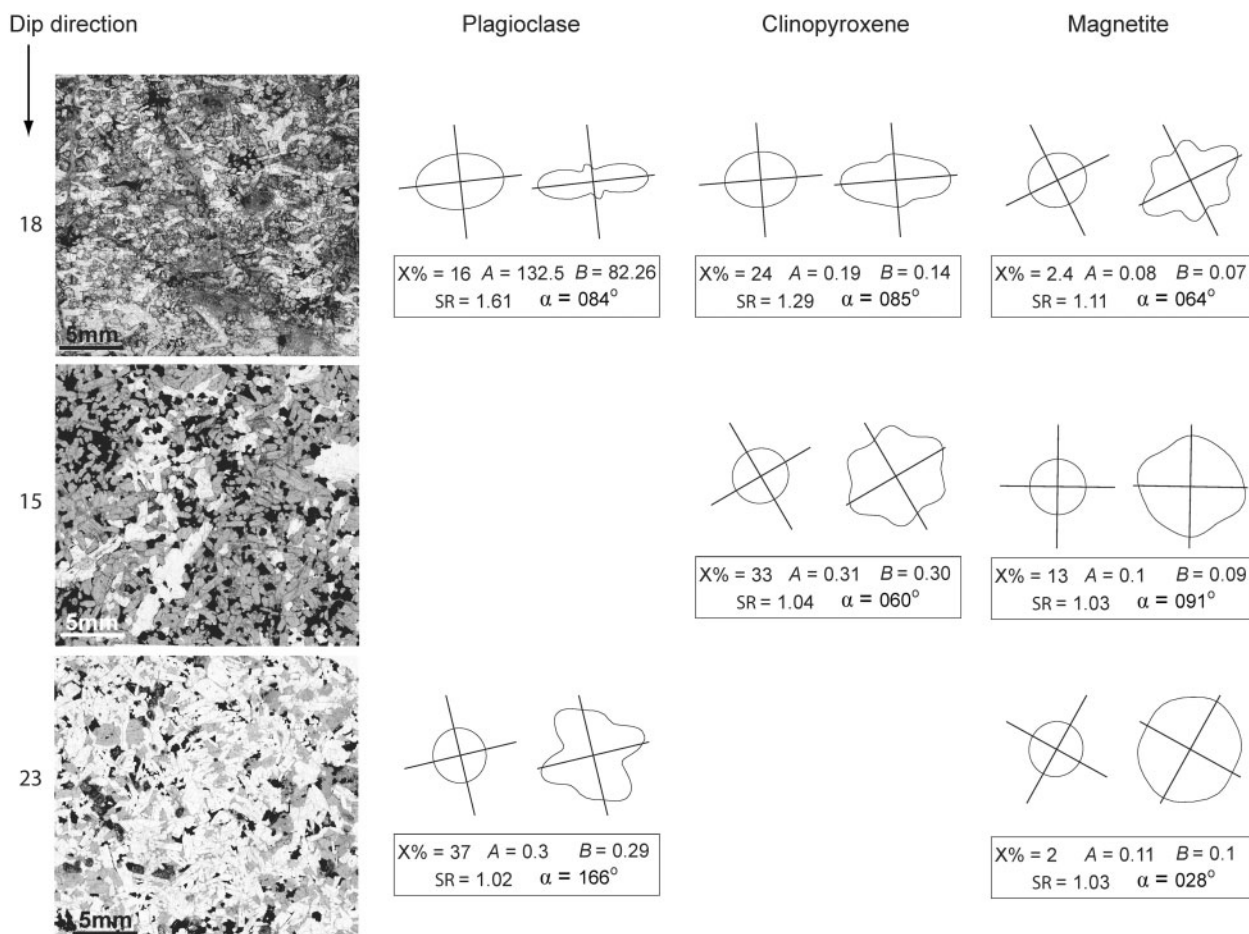


**Fig. 11.** Intercept petrofabric data for selected samples from the Druim Hain layered gabbros (see text for details). Oriented sample numbers are given and the direction of dip is arrowed.

rocks studied. This is based on the supposition of Marsh (1998) and Higgins (2002a, 2006b) that initial (unmodified) 'kinetic' textures produce straight CSDs, and that increasing curvature or kinking in CSD plot shapes reflects an increase in the complexity of the textural history of the rock.

### CSD sampling method

Thin-sections for CSD analysis were taken from the AMS blocks so that both the magnetic and intercept fabric data could be considered in the context of the overall textural history of the rocks. We focused on plagioclase feldspar for CSD analysis, as it is present as a cumulus phase in almost all of the samples studied and is the major fabric-forming mineral in most cases. CSD measurements were also made on clinopyroxene crystals for several of the Druim Hain layered gabbro samples (i.e. Samples 4, 15 and 18), where sufficient clinopyroxene is present. It was not possible to carry out CSD analysis on magnetite as the necessary numbers of crystals (>200 per sample, following Mock & Jerram, 2005) are not present. In addition,

magnetite crystal shapes are often complex and it can be difficult to separate single crystals in glomerocrysts, even in reflected light, which makes CSD work difficult. This is particularly true of the anhedral magnetite interstitial to the main cumulus framework-forming minerals (plagioclase and pyroxene) in some of the Druim Hain layered gabbro samples. Plagioclase, as an early crystallized (cumulus) mineral phase in all of the samples studied, has also potentially recorded primary magmatic processes, unlike a relatively late-crystallizing phase, such as magnetite, which in some cases has pseudomorphed the last remaining melt present. We justify linking our (plagioclase and pyroxene) CSD and petrofabric (plagioclase, clinopyroxene and magnetite) datasets based on the following textural and field observations:

(1) The Ardnamurchan laminated gabbros contain cumulus plagioclase and magnetite (although minor intercumulus magnetite also occurs). The fact that there is consistency between field, AMS and intercept fabric datasets means that the processes involved in fabric formation affected all mineral phases. Thus, although plagioclase

CSDs and microprobe data may record processes that occurred earlier in the textural history of the rock, the texture observed is interpreted as a final product that is likely to preferentially record later-stage processes, including those responsible for fabric formation, and earlier textural arrangements are likely to be overprinted.

(2) In the case of the Druim Hain laminated gabbros, thin-section observation and intercept data indicate that magnetite cannot be as confidently related to the primary plagioclase and clinopyroxene cumulus framework. This is because (a) AMS lineations are inconsistently oriented and (b) lineations exhibited by plagioclase and clinopyroxene do not agree with those for magnetite. However, AMS fabrics indicate that magnetite foliations parallel the visible lamination measured in the field; the latter is always carried by either plagioclase or clinopyroxene (or both). It will be demonstrated below that there is no relationship observed between  $H$  and  $K_{\text{mean}}$  for the Druim Hain samples (the latter acting as a proxy for the volume of magnetite), suggesting that the fabrics reflect the distribution of magnetite. Integrating the CSD data, we will show that the plagioclase and clinopyroxene cumulate framework has in some way been important in controlling the magnetic texture. Again, the assumption made is that the texture observed is the final product of all of the processes that have occurred, and that later modification is preferentially preserved.

All of the CSD analyses of the plagioclase from the Ardnamurchan laminated gabbros were carried out on thin-sections cut perpendicular to the lamination plane; plagioclase crystals in the plane of lamination often have poorly defined crystal boundaries. Six samples were analysed from the Sithean Mor laminated gabbro, two from the Achnaha laminated gabbro and five from the Glendrian laminated gabbro (see Fig. 7). Nine thin-sections were selected from the Druim Hain AMS sample suite for CSD analysis (Fig. 8). Of these, plagioclase crystals were measured for Samples 6, 8, and 23 (plagioclase-rich cumulates), and clinopyroxene crystals were measured for Samples 4 and 15 (clinopyroxene-rich cumulates). Four thin-sections were prepared from Sample 18, to analyse both plagioclase and clinopyroxene, parallel to and normal to the plane of mineral lamination.

To analyse the CSDs of the laminated gabbros, single crystals were identified and outlined on hard-copy overlays of high-resolution photomicrographs of single thin-sections. This texture overlay was then edited into a simple bitmap format before being opened in the image analysis software package UTHSCSA (University of Texas Health Science Center at San Antonio) ImageTool (see Fig. 12). The image scale was set and crystal area, orientation and long and short axis length were measured. The smallest crystals measured (at  $25\times$  magnification) were  $\sim 0.1$  mm in size. As all of the samples measured are

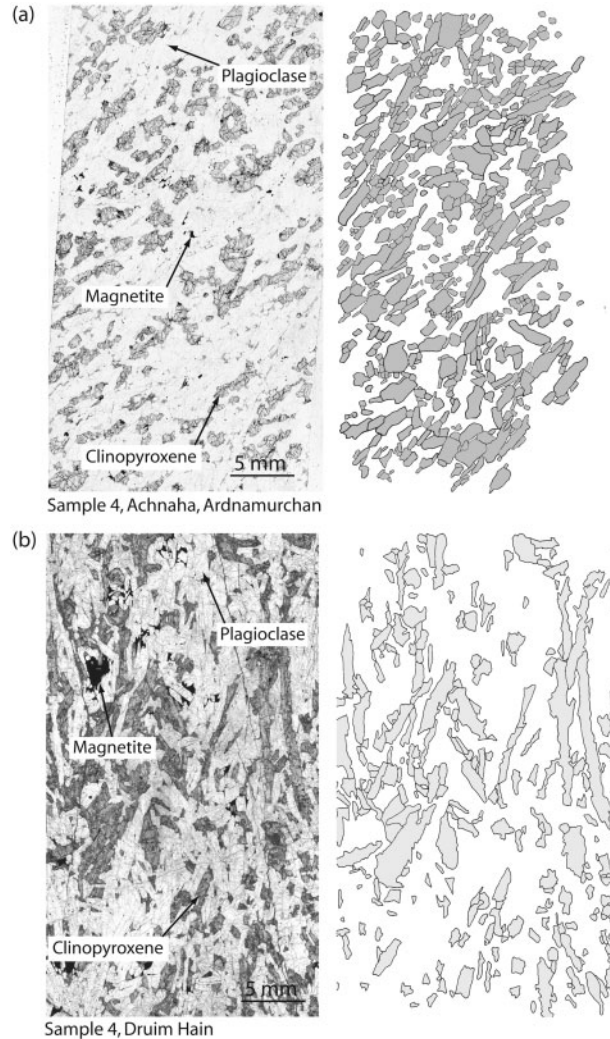


**Fig. 12.** Examples of photomicrographs and digitized texture maps for selected samples. (a) Sample 4, plagioclase CSD, Achnaha, Ardnamurchan; (b) Sample 4, pyroxene CSD, Druim Hain.

holocrystalline, it is considered that all crystals have been measured for each sample, and we therefore take the smallest grain size reported for each sample as the limit for that sample. CSD analysis was carried out as outlined by Higgins (2000, 2002b) and the size distributions of the long axes of crystals were measured and corrected for 2D–3D effects using the CSDCorrections (Version 1.37) software of Higgins (2000).

It should be noted that several CSD studies on foliated plutonic rocks have advocated caution when using measurements of the crystal long axis as the ‘crystal-size’ parameter (Launeau & Cruden, 1998; Boorman *et al.*, 2004). This is because irregularly shaped crystals and crystals with high aspect ratios can cause CSDCorrections to calculate curves with overestimated volume phase proportions or shallower slopes. To circumvent these issues,

Boorman *et al.* (2004) measured Feret length, the length of a square with the same area as that of the crystal (crystal aspect ratio and roundness are 1:1:1 and zero, respectively), whereas Launeau & Cruden (1998) measured crystal area and used the appropriate diameter of a circle as a measure of crystal size. Some of the problems associated with converting 2D crystal shapes into 3D are avoided in this way, especially for rocks containing irregularly shaped crystals. However, as stated by Boorman *et al.* (2004), 'uncertain error is introduced in the cut section and fabric correction by the assumption of cubic shape', the effect of which may cause the CSDCorrections software to output incorrect slope values. The work of Morgan & Jerram (2006) supported this by highlighting that the assumption of a spherical crystal shape gives a poor estimation of CSD slope. For these reasons, and given that mineral fabrics in our samples are strong, we have used crystal length as the size parameter for CSD analysis. To gain the most accurate CSD slope possible, mean values of crystal roundness, volume phase proportion and fabric strength for input into CSDCorrections in each sample were estimated directly from the digitized images and the thin-sections for each sample (see Higgins, 1994, 2000, 2006b; Coogan *et al.*, 2002; Jerram *et al.*, 2003; Boorman *et al.*, 2004; Mock & Jerram, 2005). In most examples studied, where CSDs were calculated from thin-sections normal to the plane of lamination, linear fabrics on the plane were considered to be sufficiently weak so as not to affect the results significantly (e.g. Higgins, 2006b).

Calculation of a crystal shape defined by a 3D aspect ratio with short:intermediate:long (S:I:L) axes, for input into CSDCorrections, from 2D thin-sections is not straightforward (Higgins, 1994, 2006b; Higgins & Chandrasekharam, 2007). Higgins (1994) formulated a model that simplified the problem by treating crystals as parallelepipeds. In this case, the mode of intersection width/intersection length (2D aspect ratio) is equal to the ratio S/I. Calculating the ratio I/L is more complicated, and simple modelling of populations of parallelepipeds has been shown to yield imprecise results for some crystal shapes (Garrido *et al.*, 2001; Higgins, 2006b). The CSDSlice program of Morgan & Jerram (2006) calculates a best fit for the 2D aspect ratios and compares these directly with curves for known crystal shapes. However, this approach places equal weight on both the S/I ratio and the I/L ratio, despite the fact that data for the latter may be less reliable. Higgins & Chandrasekharam (2007) showed that for populations of plagioclase containing an alignment of crystals, I/L could be extracted with a greater degree of confidence from oriented thin-sections: (010) faces in plagioclase tablets often lie parallel to a planar foliation, so that examination of thin-sections cut parallel to the foliation may yield I/L. Higgins (2006b) and Higgins & Chandrasekharam (2007) also suggested

that for euhedral tabular plagioclase crystals, I/L is often equal to unity.

In this study, all of the Ardnamurchan and Druim Hain samples have a well-developed planar lamination, so it is possible to quantify I/L for all of the plagioclase and pyroxene crystal populations studied by careful study of thin-sections cut parallel to the mineral lamination. These observations have revealed that choice of one aspect ratio would not suffice for all samples, and that in many cases  $S < I < L$ ; that is, crystal shapes are triaxial (see examples illustrated in Figs 10 and 11). Thus, working on the assumption that (010) faces lie in the plane of lamination in all samples studied (see above and Higgins & Chandrasekharam, 2007), we have estimated values for S/I and I/L from the modes of width/length intersection ratios estimated from thin-sections cut normal and parallel to the lamination, respectively (see Higgins, 2006b). Aspect ratios were also calculated using the numerical approach of Morgan & Jerram (2006), to compare both datasets. For most samples, reasonable values for I/L (i.e. I/L generally = 0.5) were provided by CSDSlice, but in some instances, (e.g. Samples 6, 7 and 11 from Ardnamurchan), the program miscalculated significantly (see Table 3). In the case of the Ardnamurchan laminated gabbros, an independent estimate, using a universal stage, of the overall aspect ratio of plagioclase crystals (1:1.5:4) by Fortey (1980), also suggesting a triaxial shape, is in fair agreement with the data obtained here. The crystal shapes calculated here also compare reasonably well with values obtained for 2D and 3D aspect ratios in other studies of cumulate rocks. For example, 2D ratios of 1:6 (maximum 1:14) for plagioclase in foliated gabbros of the OB-III and OB-IV zone of the Stillwater Complex were calculated by Meurer & Boudreau (1998). In a quantitative textural study of massive and foliated anorthosite in the Sept Iles layered intrusion, Higgins (1991) calculated aspect ratios for plagioclase of 1:2.5 and 1:4.8, respectively. The study of Boorman *et al.* (2004) revealed tabular plagioclase crystal shapes; aspect ratios typically were <2.5. However, Boorman *et al.* (2004) also described a strong correlation between crystal aspect ratio and the alignment factor (a measure of the strength of the petrofabric; after Meurer & Boudreau, 1998) with no lineation, and inferred significant compaction-related recrystallization.

## CSD results

CSD data for all samples are presented in Table 3 and CSD plots are illustrated in Fig. 13. The raw data output from the CSDCorrections program for all samples measured is presented in Electronic Appendix 1 (available at <http://www.petrology.oxfordjournals.org/>). Plots of CSD slope against  $L_{\max}$  and intercept ( $n_0$ ) are presented in Fig. 14 and discussed below. It should be noted that  $L_{\max}$  is measured (in mm) as the average of the four largest grains

Table 3: Quantitative textural (CSD) data (input and output) for all samples

Sample no.	Vol. phase prop.	Aspect ratio (calc.)	Aspect ratio (CSDSlice)	Roundness	CSD slope	$\ln(n_0)$	$n_0$	No. of crystals	$R^2$	$L_{\max}$ (mm)
<i>Ardnamurchan</i>										
1	52	1:1.67:3.33	1:1.5:2.7	0.6	-0.38	-3.29	0.04	189	0.99	11.18
4	45	1:1.67:3.33	1:1.6:3.6	0.6	-1.08	0.84	2.31	692	0.99	4.26
5	32	1:2.5:5.0	1:2.3:3.6	0.6	-0.66	-1	0.37	379	0.97	6.53
6	45	1:3.33:6.67	1:2.3:9.0	0.6	-0.94	0.98	2.68	377	0.99	4.09
7	47	1:3.33:6.67	1:2.7:8.0	0.5	-1	1.32	3.74	350	0.97	4.46
9	49	1:2.0:4.0	1:1.9:3.8	0.6	-1.24	1.53	4.63	248	0.95	3.46
10	43	1:2.0:4.0	1:1.7:2.8	0.6	-1.5	2.02	7.56	338	0.99	3.57
11	48	1:2.5:5.0	1:1.15:9.0	0.6	-0.97	1.05	2.85	135	0.97	2.88
13	42	1:2.5:5.0	1:1.5:4.0	0.6	-0.87	0.14	1.15	241	0.98	4.45
15A	36	1:1.67:3.33	1:1.6:2.9	0.6	-0.99	0.18	1.2	187	0.99	4.49
17A	45	1:1.67:3.33	1:1.3:2.9	0.6	-1.05	0.59	1.8	313	0.98	4.2
19	54	1:3.33:6.67	1:1.6:3.6	0.5	-0.92	1.08	2.94	606	0.98	4.85
22A	56	1:2.0:4.0	1:2.0:4.5	0.6	-1.15	1.54	4.67	326	0.98	3.86
<i>Druim Hain</i>										
4	29	1:3.33:5.56	1:2.4:6.0	0.5	-0.6	-1.32	0.27	278	0.91	9.19
6	27	1:2.5:6.25	1:1.6:3.6	0.6	-1.5	2.72	15.2	1191	0.99	2.57
8	38	1:2.0:5.0	1:1.4:4.5	0.6	-1.52	2.83	16.95	642	0.99	2.84
15	29	1:1.25:2.1	1:1.15:1.6	0.6	-1.44	0.76	2.13	270	0.94	3.66
18AP	20	1:3.33:6.67	1:3.2:5.5	0.5	-1.64	2.12	8.29	628	0.99	2.98
18APY	30	1:2.5:4.2	1:1.3:2.1	0.6	-1.39	1.36	3.9	688	0.97	3.88
18BP	20	1:3.33:6.67	1:3.2:7.0	0.5	-1.21	0.83	2.28	449	0.99	3.75
18BPY	25	1:2.5:4.2	1:1.8:4.5	0.5	-1.45	0.8	2.22	305	0.99	5.71
23	53	1:3.33:6.67	1:2.1:5.0	0.5	-0.74	0.37	1.45	1028	0.95	6.76

from the crystal population of each sample (e.g. Boorman *et al.*, 2004; O'Driscoll *et al.*, 2007a).

#### *Ardnamurchan laminated gabbros*

Although there is some variation in the CSD plots (Fig. 13a–c) for different samples, all of the CSD curves display approximately log–linear relationships for larger crystal size fractions. Linear regression by the least-squares method was carried out in Microsoft Excel on the larger crystal size fraction of each plot. None of the curves have an  $R^2$  value of less than 0.95. Measured slope values are relatively steep (–0.8 to –1.5). The exceptions are Samples 1 and 5, with measured slope values of –0.38 to –0.66, respectively. Samples 5, 6, 9, 15 and 17 display pronounced ‘humped’ profiles at small size fractions, whereas the remainder of the samples are approximately log–linear through the entire range of sizes.

#### *Druim Hain layered gabbros*

*Plagioclase.* CSD results for plagioclase in the Druim Hain gabbros (Samples 6, 8, 18 and 23) are fairly

consistent (Fig. 13d and e). The CSD plots reveal log–linear distributions for large size fractions in all cases ( $R^2 \geq 0.91$ ). Slope values are also well constrained, in the range –1.2 to –1.6, with the exception of the shallow slope exhibited by Sample 23 (–0.74). All samples exhibit slightly humped profiles at small size fractions. It should be noted that the CSD data from the sections normal and parallel to the mineral lamination for plagioclase in Sample 18 show good agreement; there should be only one mean CSD for any sample (Higgins, 2006b).

*Clinopyroxene.* As with the crystal shape data, the CSDs for clinopyroxene in the Druim Hain layered gabbros are similar to those for the plagioclase data and are log–linear at large size fractions ( $R^2 \geq 0.91$ ) (Fig. 13e and f). CSD slopes for Samples 4 and 15 are –0.6 and –1.4, respectively. Again, CSDs for sections cut normal and parallel to the mineral lamination in Sample 18, this time for clinopyroxene, show good agreement. Mildly humped profiles are observed at small size fractions for all plots. A subtle deviation from a straight-line plot is observed around the 4–7 mm size interval for Samples 4 and 15, where the plot is concave upward.

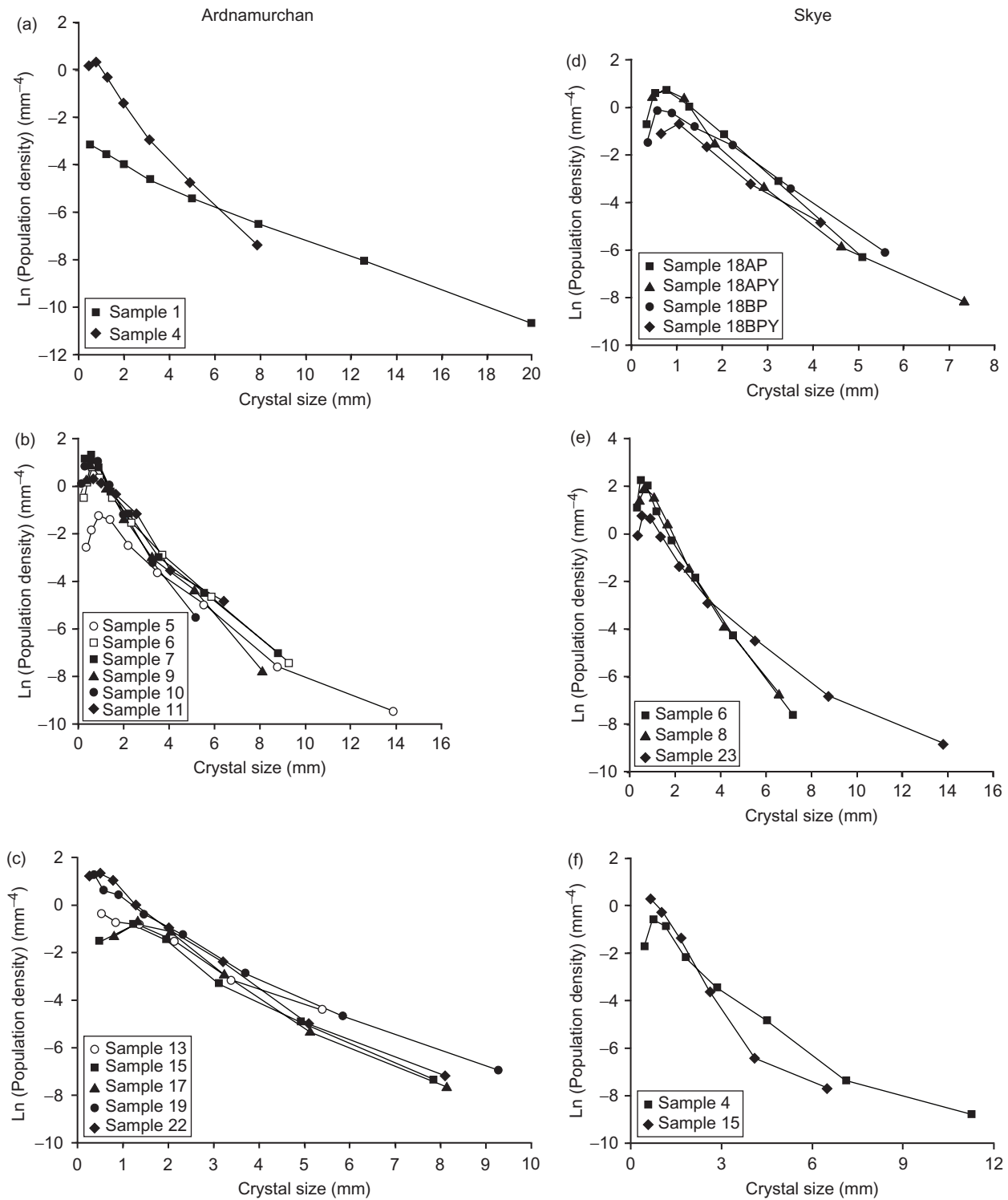


**Fig. 13.** CSD plots for all samples grouped by sample location. (a), (b) and (c) are the Achnaha, Glendrian and Sithean Mor samples, respectively. (d) CSDs for Sample 18; 18A and 18B are measurements parallel and normal to the plane of lamination, respectively. P and PY are for plagioclase and pyroxene CSDs, respectively. (e) Plagioclase CSDs from the Druum Hain layered gabbros. (f) Clinopyroxene CSDs for the Druum Hain layered gabbros. (See text for further discussion.)

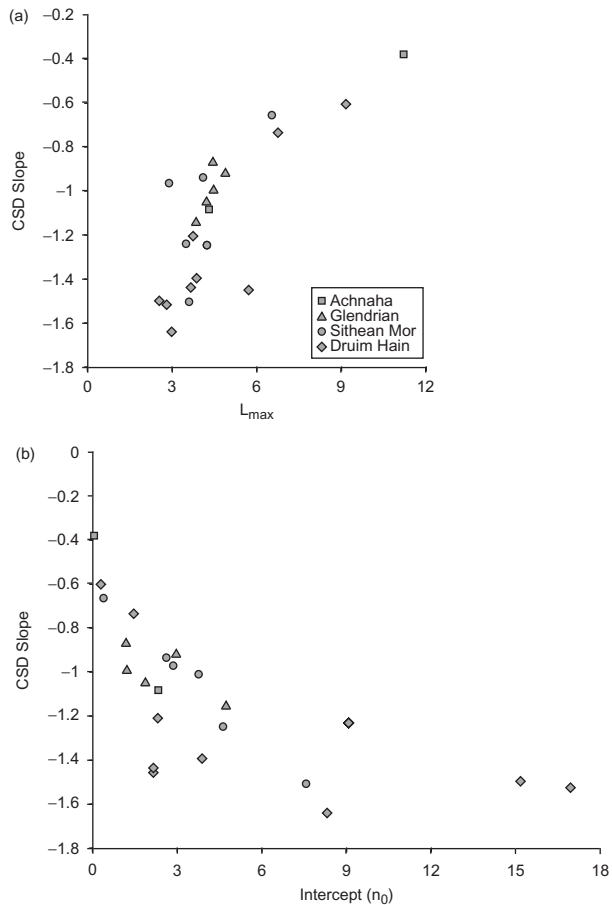


**Fig. 14.** Plots of (a) CSD slope vs  $L_{max}$  and (b) CSD slope vs intercept ( $n_0$ ).

## MAJOR ELEMENT PROFILING OF PLAGIOCLASE

Major element concentrations of plagioclase phenocrysts were measured on a Cameca SX-50 electron microprobe at IFM-GEOMAR, applying the built-in PAP correction procedure (Pouchou & Pichoir, 1984). Analytical conditions included an acceleration voltage of 15 kV, a beam current of 8–20 nA and counting times of between 20 and 60 s on peaks. A rastered beam of  $3 \mu\text{m} \times 4 \mu\text{m} = 12 \mu\text{m}^2$  was used for feldspar to minimize Na loss. Na counts were continuously monitored during analysis and generally remained stable over at least twice the measurement time. Relative analytical precision [(standard deviation/mean)  $\times 100$ ] was  $<2\%$  for Si, Al, and Ca,  $<3\%$  for Na and K,  $<4\%$  for Ti,  $<5\%$  for Fe and  $<10\%$  for Mg, based on repeated analysis of natural and synthetic mineral and glass standards.

Four plagioclase crystals from each of two samples of laminated gabbro (Sample 5 from Ardnamurchan and Sample 18 from Druim Hain) were selected to test for major element sub-crystal zonation, to provide a better

constraint on the textural and AMS data. Sample 5 was selected for microprobe analysis as it is the only sample of the AMS–CSD suite from the Sithean Mor that exhibits visible magmatic layering as well as a strongly developed layer-parallel mineral lamination. Approximately 200 points per crystal were analysed along a rim-to-rim traverse with spot distances of between 22 and  $34 \mu\text{m}$ . Sample 18, from Druim Hain, a well-laminated plagioclase- and clinopyroxene-bearing cumulate, was selected for microprobe analysis and  $\sim 100$  points (rim-to-rim) were analysed per crystal with spacing between 43 and  $54 \mu\text{m}$ . In both cases, thin-section observation revealed the presence of mineral and melt inclusions in the data ( $\sim 4$ – $5$  points per crystal), which have been removed from the plots presented here. The data measured from both localities are presented in Electronic Appendix 2.

## Results

### *Ardnamurchan laminated gabbros*

Figure 15 summarizes the microprobe data for plagioclase from Sample 5. An mol% is plotted against (rim-to-rim) distance for each of the crystals analysed (Fig. 15a). Anorthite contents for the four crystals typically are in the range  $An_{50-75}$  (although exceptions outside these values are observed) with inter-crystal variation of up to  $\sim 30$  An mol%. The  $K_2O$ – $CaO$ – $Na_2O$  ternary system is also shown for all crystals in Fig. 15b, confirming this range of compositions. The trend shown by Traverses 1, 2 and 4 and, to a lesser extent, by Traverse 3, has a lower An core, always with several more well-defined overgrowth zones, ending with a low An rim (Fig. 15a). Values of  $\Delta$ An mol% between any two given data points defining these regular zones can be up to 10%, indicating marked changes in chemical composition.

### *Druim Hain layered gabbros*

Figure 16 summarizes the microprobe data for plagioclase from Sample 18. The graphs illustrate An mol% plotted against (rim-to-rim) distance for each of the crystals analysed (Fig. 16a). Anorthite contents for the four crystals range between approximately  $An_{55}$  and  $An_{65}$ , typically with less than 5% An variation between any two data points. The maximum  $\Delta$ An% between any two given data points is  $\sim 7\%$ . However, although irregular rim-to-rim variation is observed in each crystal, evidence of systematic compositional zones is not present, in contrast to Sample 5 from Ardnamurchan described above. The  $K_2O$ – $CaO$ – $Na_2O$  ternary system for each crystal is also plotted in Fig. 16b, and shows that all four are relatively similar in composition, compared with the Ardnamurchan data. [It should be noted that these data are broadly consistent with Wager & Brown's (1968) observation that plagioclase on Druim Hain ranges in composition between  $An_{58}$  and  $An_{69}$ ]

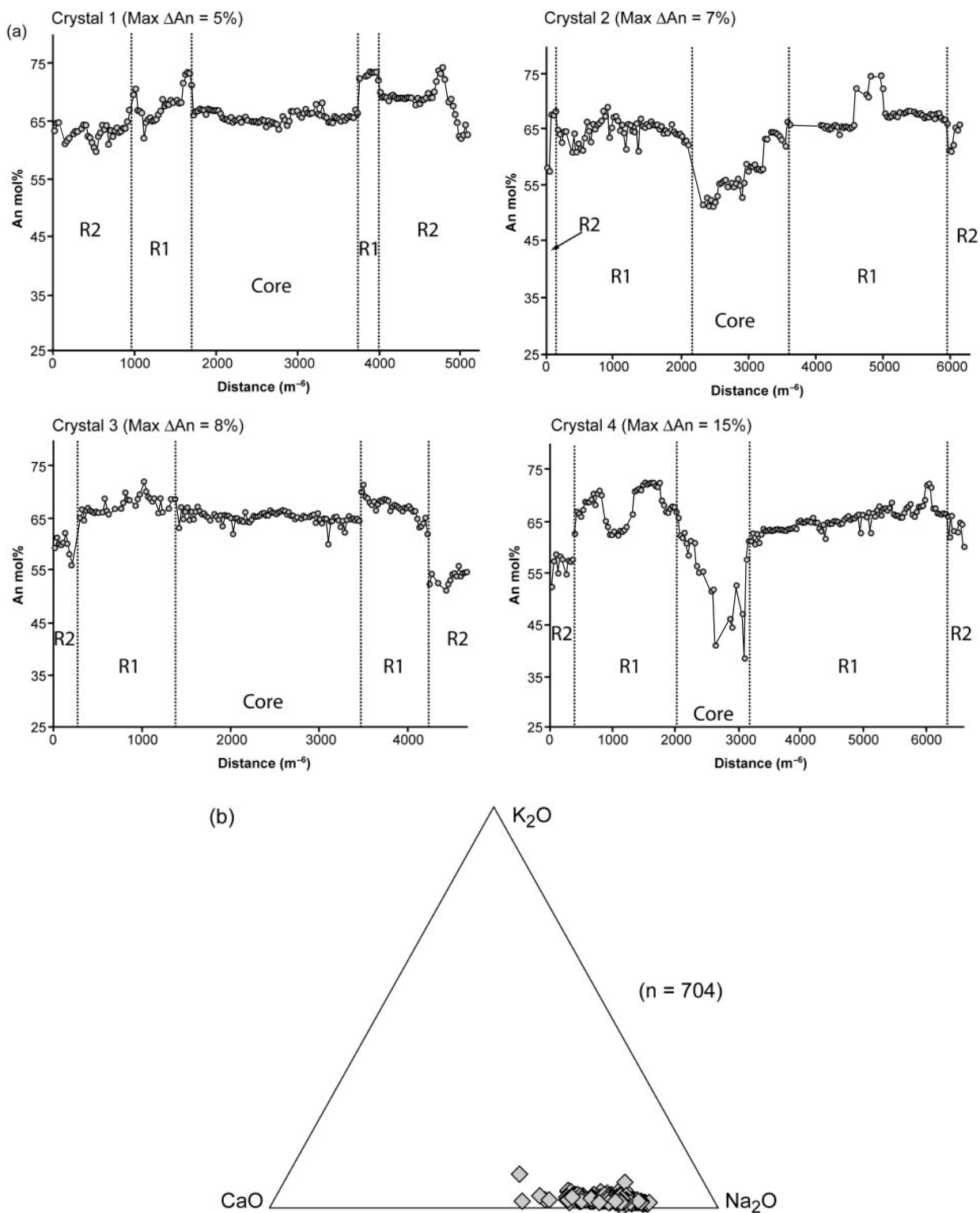


**Fig. 15.** (a) Plots of An mol% against distance for rim-to-rim traverses of four plagioclase crystals from Sample 5, Ardnamurchan. The maximum  $\Delta An$  change between any two data points is given in each case. (b) Ternary  $K_2O$ - $CaO$ - $Na_2O$  plot illustrating mineral compositions for all four plagioclase crystals analysed.

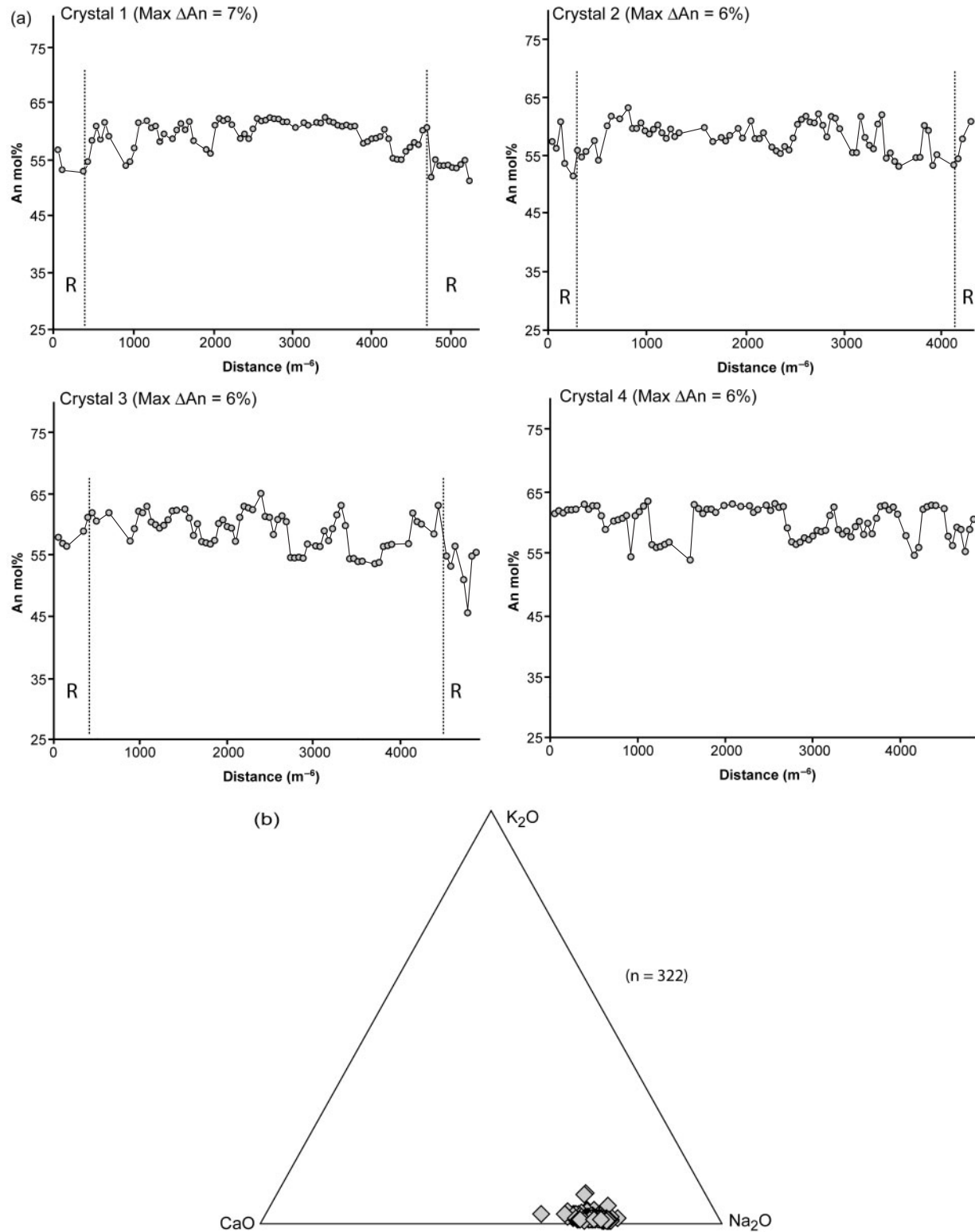


**Fig. 16.** (a) Plots of An mol% against distance for rim-to-rim traverses of four plagioclase crystals from Sample 18, Druim Hain. The maximum  $\Delta An$  change between any two data points is given in each case. (b) Ternary  $K_2O$ - $CaO$ - $Na_2O$  plot illustrating mineral compositions for all four plagioclase crystals analysed.

## DISCUSSION

### Development of the Ardnamurchan laminated gabbro

#### *Inferences from petrofabric data*

Magnetic foliations in the laminated gabbros are well developed and consistently parallel to the mineral lamination observed in the field. Thus, the AMS foliations are an accurate reflection of the visible fabric. In addition, the intercept petrofabric data presented in this study indicate that the AMS lineations, carried by the shape preferred orientation (SPO) of magnetite crystals (see the Appendix), correspond well to linear arrangements of plagioclase crystals on mineral lamination planes. The AMS lineations are well constrained and in almost all samples from the Glendrian and Achnaha laminated zones, and several from Sithean Mor, plunge consistently downdip (inward) on magnetic foliation planes (Fig. 7). Independent supporting evidence of these findings has been provided by Fortey (1980), who presented measurements of the crystallographic preferred orientations (CPO) of plagioclase grains on mineral lamination planes in five samples from the Achnaha, Sithean Mor and Glendrian bodies using the universal stage. Fortey (1980) used a similar technique to that described by Brothers (1964) for the laminated troctolites of the Eastern Layered Series, Rum. [See also O'Driscoll *et al.* (2007b), who found that AMS fabrics correlated well with the universal stage CPO data from laminated cumulates of the Rum Layered Suite, NW Scotland, published by Brothers (1964).] Fortey (1980) found that in four of his five samples, the plagioclase lineations were oriented downdip on mineral lamination planes, and in one Glendrian sample, oriented parallel to strike of the lamination. Although Fortey used a very small number of samples, his results led him to concur with the previous studies (Richey & Thomas, 1930; Bradshaw, 1961; Wills, 1970) that lamination development was a result of emplacement-related primary flow of a crystal mush.

There have been several studies on mafic intrusions that have shown the importance of late-stage (postcumulus) movement of unconsolidated cumulate, rather than primary emplacement-related magma flow, to the development of mineral fabrics (e.g. Higgins, 1991; McBirney & Nicolas, 1997; O'Driscoll *et al.*, 2007b). The presence of well-developed, directionally consistent lineations carried by both plagioclase and magnetite rule out fabric formation as a result of processes that might produce a planar fabric only, such as crystal settling, *in situ* crystallization or compaction (although the involvement of these processes is not ruled out completely). However, a paucity of evidence of solid-state deformation suggests that compaction-related processes were not influential at a late stage in the crystal mush. In addition, the fabrics in the Ardnamurchan laminated gabbros are not considered to

have resulted from alignment of plagioclase or magnetite seed crystals in a flowing melt (i.e. emplacement related). Instead, it is considered that the linear and planar fabrics result from shearing and syn-magmatic deformation of a layered crystal mush. This notion is favoured because of the parallelism of the planes of magnetic foliation, mineral lamination and magmatic layering, the syn-magmatic deformation of this layering, and the downdip orientation of magnetite and plagioclase lineations. The mineral lamination and AMS fabrics in the laminated gabbros probably reflect convergent flow of unconsolidated cumulate during slumping and shearing of a crystal mush, a process similar to that described for foliated anorthosite in the Sept Iles intrusion (Higgins, 1991) and for the laminated Rum Eastern Layered Series cumulates (O'Driscoll *et al.*, 2007b). The crystal aspect ratio data presented here indicate that the crystals forming the laminated rocks are variably triaxial or prismatic in shape, rather than tabular; the latter might be expected if magmatic flow had formed the lamination, with poorly sorted crystal shapes resulting from more chaotic slumping processes. It is envisaged that deformation of layering and mineral fabric development probably occurred during inward tilting and rotation of layer planes toward the centre of the intrusion, in a manner similar to that proposed for the layering and AMS lineations in the Great Eucrite gabbros by O'Driscoll *et al.* (2006) and O'Driscoll (2007); that is, constrictional flow of unconsolidated cumulate. The inward-plunging AMS lineations and plagioclase lineations thus plausibly represent a stretching lineation related to centrally directed sagging of the Ardnamurchan Centre 3 gabbros. This is supported by the fact that syn-magmatically deformed layering gives slumping (sense of shear) directions consistent with the plunges of the AMS lineations. Finally, although most of the samples from the Sithean Mor laminated gabbro do not have similarly oriented inward plunging magnetic lineations to those described above, it is interesting to note that Samples 5 and 6, the only samples from well-layered localities (which also exhibit syn-magmatic deformation of layering) on Sithean Mor, have centrally plunging magnetic lineations.

#### *Textural history of the Ardnamurchan laminated gabbros*

Petrographic examination of the Ardnamurchan laminated gabbros reveals the presence of cumulus plagioclase and clinopyroxene. Magnetite is thought to occur both as cumulus and intercumulus material, based on crystal shapes and distribution. Although the Ardnamurchan gabbros preserve strong evidence for fabrics that are interpreted to have formed in the crystal mush (i.e. mobilization and slumping of crystal mushes), the textures are suggestive of widespread, sometimes subtle, late-stage modification. Irregular grain boundaries sometimes cause 'stubby' plagioclase crystals to have an almost consertal-type intergrown texture meaning that straight crystal

edges are often lacking. Examination of dihedral angles between plagioclase–plagioclase–clinopyroxene triple junctions show that they are higher than values for inherited impingement textures (e.g. Holness *et al.*, 2005; M. B. Holness, personal communication, 2007), suggesting a certain amount of sub-solidus overgrowth at grain boundaries. It is notable that little or no evidence of compaction-related crystal plastic strain is observed in these rocks (see McBirney & Nicolas, 1997; Boorman *et al.*, 2004) even where crystal aspect ratios are high.

All of the 13 CSD plots for the Ardnamurchan laminated gabbros (Fig. 13) exhibit fairly straight (log–linear) CSDs for most crystal size fractions, suggesting a simple crystallization history of just one crystal population (Cashman & Marsh, 1988). Plots of CSD slope vs  $L_{\max}$  and intercept, which show positive and negative trends, respectively, are also consistent with the notion that the laminated gabbros nucleated and grew as one crystal population (Fig. 14a and b; see Marsh, 1998). The Sithean Mor and Glendrian samples yield fairly consistent results; similar CSD slopes are observed for the main portion of the plot for all samples, although Samples 1 and 4 from Achnaha exhibit markedly different slopes (Fig. 13a). Some CSDs have a distinct convex-upward profile at small crystal sizes; for example, Samples 5, 6 and 9 from Sithean Mor and Sample 15 from Glendrian. This is not believed to be an artefact of the measurement process, as all crystals have been analysed in the samples. Rather, it might be suggestive of textures in the laminated gabbros having undergone some postcumulus growth or modification of large crystals at the expense of smaller ones (i.e. Ostwald ripening, Marsh, 1998; Boorman *et al.*, 2004). In laminated cumulates such as these, this type of profile might also suggest a significant loss of nuclei (small size fractions) by expulsion of liquid through the crystal mush (Marsh, 1988), perhaps as a result of compaction, although this process is not believed to have been significant in these rocks for the reasons outlined above.

Although all of the CSD plots have been described as being approximately log–linear, many display subtle kinks at varying larger size fractions, in most cases to shallower slopes (e.g. Samples 5 and 13), as described above. This suggests that the crystal population deviates to a proportionally greater number of larger size fractions than predicted by a log–linear distribution. These kinks are probably not substantial enough to indicate the presence of a wholly different crystal population, but may be sufficient evidence for slight ripening of some crystals to somewhat larger sizes in addition to overturning of CSD plot-shapes at small size fractions. To examine this process of textural ripening further for the laminated gabbros we have plotted the degree of strength ( $H$ ) of our AMS fabrics against both  $K_{\text{mean}}$  and CSD slope (Fig. 17a and b). The rationale for plotting these parameters is that any change

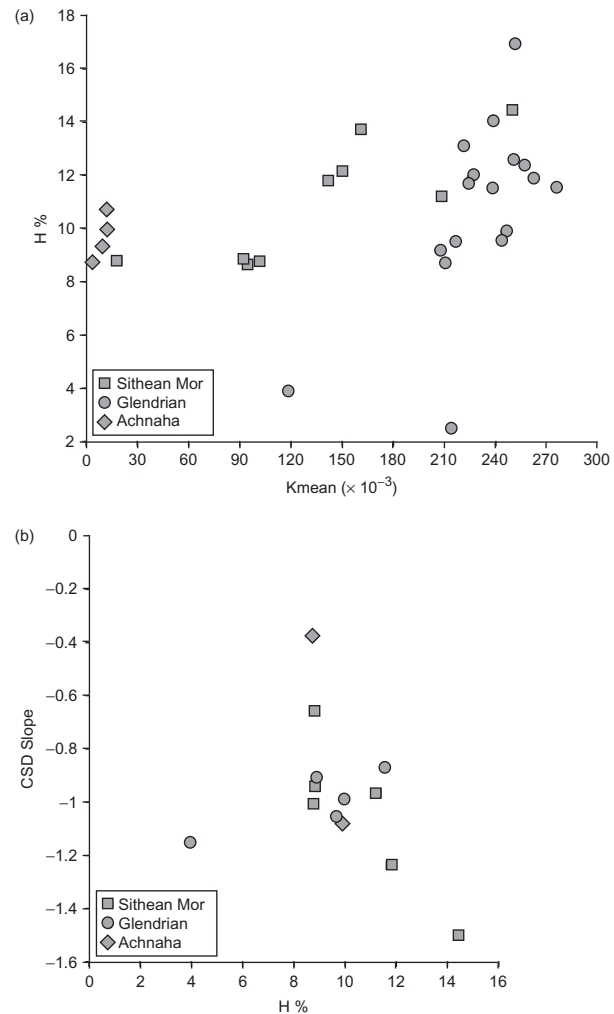


**Fig. 17.** Ardnamurchan laminated gabbro plots of (a)  $H$  vs  $K_{\text{mean}}$  and (b)  $H$  vs CSD slope. (See text for discussion.)

in slope, which could be taken to suggest textural modification (see below), could be related to fabric strength, as indicated by the AMS data. Correspondence between the AMS and other datasets has already been noted for both the Ardnamurchan (correspondence between  $L$  and  $S_R$  values) and Druim Hain (correspondence between higher values of  $F$  and the grain size of plagioclase and clinopyroxene) samples. The plot of  $H$  vs  $K_{\text{mean}}$  shows a positive trend for all of the laminated gabbro zones, and may indicate a dependence of the strength of the AMS anisotropy on the volume of magnetite present. Given that a significant proportion of the magnetite is cumulus, the consistency of the fabric orientations at an intrusion scale and the good correlation between the AMS and intercept count datasets, this positive trend might suggest that the AMS fabrics reflect processes that simultaneously affected all fabric-forming mineral phases in the crystal mush (i.e. plagioclase, clinopyroxene and magnetite). The plot

of CSD slope vs  $H$  reveals a reasonable negative correlation, suggesting that as CSD slope becomes shallower the strength of the anisotropy decreases. This is interesting considering Higgins' (2002a) CSD analyses of plagioclase cumulates in the Kigaplait intrusion, in which he highlighted that with increased textural ripening, CSD plots tend to shallower slopes. In this light, our data would thus seem to suggest that with increased textural ripening, the strength of the fabric is weakened, an effect that has been noted by Higgins (1998) in the Lac-St-Jean anorthosite complex, Canada. The plot of CSD slope vs  $H$  exhibits one significant outlier (Sample 1). The locality from which this sample was obtained is one where significant syn-magmatic deformation is observed. In this case, it is possible that mixing of primocrysts from different cumulate layers as a result of destabilization of sequences of unconsolidated, layered cumulate has been the cause of the observed CSD plot shapes and petrofabrics observed. Several samples from Sithean Mor have magnetic lineations that deviate from a downdip orientation. It is difficult to explain this with the current dataset, but it is not believed that the anomalously oriented lineations are a product of extreme sub-solidus fabric degradation, as these are well-defined (internally consistent) AMS fabrics and concentrically zoned plagioclase is preserved in most samples. O'Driscoll (2007) suggested that mineral lamination planes at Sithean Mor that dip more steeply ( $70\text{--}80^\circ$ ) inward than the Glendrian and Achnaha laminated gabbros ( $20\text{--}30^\circ$  and  $50\text{--}55^\circ$ , respectively), together with their peripheral position, might suggest they represent an older body. This in turn may indicate a more protracted super-solidus textural (postcumulus) history than in the inner Glendrian and Achnaha bodies.

Elemental profiles of plagioclase phenocrysts from Ardnamurchan reveal distinct zonation of anorthite content, indicating a complex 'pre-cumulus' history of growth and disequilibrium conditions reflected by sharp compositional changes. All of the crystals have a somewhat more sodic core that grades out through some more calcic zones, to a narrow outer rim of complicated small-scale variation. The maximum  $\Delta An$  in these crystals (between any two data points) is up to 10 mol%, suggesting that all four crystals have experienced variable chemical environments (i.e. host liquids; Pearce & Kolisnik, 1990). The outer, more complex rim, is likely to reflect late-stage overgrowth from rapidly changing liquids, possibly suggesting intercumulus processes where rapid depletion and unsteady supply of melt resulted in variable growth rates and conditions. It is possible that significant disruption of a layered crystal mush, as evidenced by many of the outcrops in the field, would promote mobility of the interstitial melt, bringing the crystals into contact with liquids of significantly different composition (as in the mixed crystal slurries shown in Fig. 2c), that could

give rise to the complex zoning observed in the outer parts of all four of the crystals analysed in Sample 5 (e.g. R2 in Fig. 15a).

As described above, the field evidence of syn-magmatic deformation and downdip orientations of all of the fabric datasets are strongly suggestive that the fabrics formed in a mobilized crystal mush. The simple 'straight' CSD plots at most crystal size fractions and relatively consistently oriented AMS fabrics (lineations) of the laminated gabbros indicate that, despite the evidence for zoning provided by the plagioclase compositions, only one crystal population was involved in the textural evolution of the rocks. As described above, the studies of Higgins (2002a) and Boorman *et al.* (2004) argue that textural ripening, whether driven by compaction-related processes or not, requires the presence of melt, and the latter study showed how this ripening was sufficient to markedly enhance the intensity of the fabric. The degradation of the straight crystal boundaries, high observed dihedral angles, irregular zoning at outer crystal margins and evidence for subtle degradation of the fabric (Fig. 17b) are taken as evidence that late-stage overgrowth on plagioclase crystal margins occurred. This textural adjustment process, not significant enough to destroy the concentric zoning, is believed to have been sufficient to subtly weaken or degrade, but not destroy, the quality of the fabrics in these rocks. Holness *et al.* (2007) has described how the presence of thin melt films in cumulates can facilitate permeability at vanishingly low volumes of melt, and it is considered that this was possible in the Ardnamurchan laminated gabbros as large quantities of intercumulus material are not observed in any of the samples.

## Development of the Druim Hain layered gabbros

### *Inferences from petrofabric data*

The principal differences between the Druim Hain magnetic fabrics and those from Ardnamurchan are the presence of higher anisotropies ( $H$ ) that are also rather oblate. The lack of a consistently radially inward plunging lineation orientation (double-sampled sites show that magnetic lineations are inconsistent even at the scale of a single block sample; e.g. Sample 2, see Fig. 8) is also significant and is discussed in more detail below. Otherwise, AMS data alone provide no further insight into the fabric-forming processes in the Druim Hain rocks. When the AMS data are considered with the intercept data, the unreliability of the lineation orientations is confirmed; no correlation is observed between the two datasets.

### *Textural history of the Druim Hain layered gabbros*

Thin-section observations suggest a different textural history for the Druim Hain layered rocks than for the Ardnamurchan laminated gabbros. Straight cumulus crystal boundaries and clean well-defined intercumulus crystals

indicate inherited-unmodified impingement textures (Holness *et al.*, 2005). Although a detailed universal stage dataset, calculating mean and standard deviation values of the dihedral angle populations in a sample, is required to accurately quantify igneous texture in this way (Holness *et al.*, 2005), observations on thin-sections made here suggest that plagioclase–plagioclase–clinopyroxene and clinopyroxene–clinopyroxene–magnetite apparent dihedral angles are typically lower than for the Ardnamurchan laminated gabbros ( $\leq 60^\circ$ ). Other petrographic aspects of the textures of the Druim Hain samples include evidence in the coarser-grained, more strongly foliated samples (4, 15 and 23) for solid-state deformation (described above), and minor overgrowth on cumulus magnetite crystals in magnetite-rich samples (which postdates the solid-state compaction-related deformation).

For the Druim Hain CSD plots, relatively straight-line profiles at large size fractions are observed, again suggesting the presence of a single crystal population. As with the Ardnamurchan CSD dataset, the plots of slope vs  $L_{\max}$  and intercept for Druim Hain show trends that support this interpretation, based on the modelling of Marsh (1998; Fig. 14a and b) and suggest 'batch' or closed-system crystallization.

There is a considerable degree of internal variation within the dataset, however, based on CSD slope. In the case of plagioclase, Samples 6, 8 and 18 exhibit relatively steep slopes, whereas the coarser-grained Sample 23 exhibits a significantly shallower slope. For the pyroxene CSDs, Samples 15 and 18 show relatively steep slopes whereas the coarser-grained Sample 4 reveals a shallower slope. Most of the CSD plots exhibit an overturn at small crystal sizes; as with the Ardnamurchan data this is interpreted as reflecting a loss of small crystal sizes as a result of textural ripening or expulsion of nuclei during compaction, rather than an artefact of measurement. Petrographic observation suggests that the latter process was more likely to have been significant in some of the Druim Hain rocks than for Ardnamurchan. Samples 4, 15 and 23 all exhibit significant kinks at large size fractions; these are the coarser-grained most strongly foliated samples (an observation supported by the high H values for these samples; Table 2), and also those that exhibit the best evidence of solid-state deformation.

Although secondary (postcumulus) processes such as compaction may have been significant in some samples (e.g. 4, 15 and 23), they cannot be held exclusively responsible, and some primary mechanism must be held to account for lamination development. The reason for this is that the CSD plots of many of the laminated samples measured for both plagioclase and pyroxene [e.g. Samples 6, 8 and 18 (Sample numbers 1–4)], are not kinked and are straight at the larger size-fraction portions of the curves. However, the absence of a consistent lineation at the intrusion scale

means that it is more difficult to suggest what primary process this might be than for the Ardnamurchan laminated gabbros. Both the AMS and intercept data show that the Druim Hain rocks contain some evidence of linear fabrics. However, they are always very weak and in the case of the double-sampled sites, not even consistent at the block sample scale (e.g. 2 and 13). It should be noted that the AMS data for Sample 4 shows confidence ellipses for the  $K_1$  and  $K_2$  axes of the AMS ellipsoid that almost overlap (Fig. 8), suggesting very little difference between both axes and possibly suggesting that axis switching may have occurred when considered in light of the intercept data (i.e. these are intermediate fabrics e.g. Ferré, 2002). This phenomenon arises when  $K_1 \approx K_2 > K_3$ ; that is,  $K_1$  and  $K_2$  are so similar that the sensitivity of the Kappabridge instrument is not sufficient to satisfactorily differentiate between the two. Based on these data, we take the degree of lineation in these rocks as negligible in terms of being able to interpret fabric-forming processes, given the relative strength of the foliation. We believe that the marked deficiency in small-scale structures in the layered rocks at Druim Hain supports the notion that 'sedimentary-type' processes or dynamic mobilization of unconsolidated cumulate that might have created linear fabrics were limited.

Primary magma chamber processes that can form a planar fabric without a linear fabric include (gravitational) crystal settling of tabular and tabular–prismatic crystals (see Wager & Brown, 1968) or *in situ* crystallization. The ability of plagioclase crystals, which have demonstrably lower densities than mafic silicate melts, to settle, has long been questioned; the 'plagioclase flotation problem' (McBirney & Noyes, 1979; Morse, 1979; Boudreau & McBirney, 1997). It is beyond the scope of the current study to enter this debate without further evidence, but we emphasize that the lack of modal or size grading of cumulus crystals at Druim Hain suggests that crystal settling was not influential in fabric formation. This is consistent with the comparative lack of complex pre-cumulus growth and resorption history in plagioclase zoning in Sample 18. Instead, we suggest that a slowly advancing solidification front with shallow diffusion and temperature gradients may have controlled the direction of crystal growth parallel to planes of equal chemical potential at the melt–crystal mush interface [in a manner suggested by McBirney & Noyes (1979)]. Oscillatory changes in the proportions of nucleating phases along a cotectic would give rise to the layering of different minerals. We suggest that the validity of this suggestion is supported by the very fine (centimetre) scale at which layering occurs (e.g. Fig. 2d). To invoke magmatic sedimentation for every one of these well-laminated layers in a 400 m thick sequence would be unrealistic, as it would require a separate density current to account for every layer formed.

It is also proposed that crystallization of the Druim Hain gabbros progressed upward; the presence of dropstones deforming layering close to the inferred roof of the intrusion confirms that a magma–crystal mush interface must have existed while layering was developing. The latter observation supports the inference made here that layer formation in these rocks was primary, and did not result from postcumulus processes.

Microprobe analyses for Sample 18 show that plagioclase phenocrysts lack the well-defined zoning that characterizes the Ardnamurchan samples and  $\Delta An$  is typically  $\leq 5$  mol%. The early growth history of three of the four crystals is marked by small-scale fluctuations of the supplied liquid, rather than the more dramatic and regular changes of the host liquid observed in the Ardnamurchan feldspars. It appears that the internal parts of all four crystals have a rather uniform composition ( $\sim An_{55-65}$ ) grading into more complicated zoning near the rims. We take this to reflect a stable growth situation with some late-stage overgrowth in a slightly more variable chemical environment (i.e. supply of rapidly changing liquids). This supports the notion outlined above, based on the CSD data, that distinct growth and/or ripening events in the crystallizing Druim Hain cumulate pile were probably not ubiquitous for most of their growth history, but also suggest that chemical equilibration of the crystal mush was limited as the outer zones do show some additional An variation. Had significant postcumulus modification and complete equilibration occurred, even minor chemical variation might be completely obliterated.

If the same arguments as for Ardnamurchan hold here, then the CSD data suggest that crystallization was relatively simple without the addition of foreign crystal or nuclei populations, with some samples showing the effects of subsequent crystal ripening of plagioclase and clinopyroxene. As only three of six samples have CSDs that show evidence for significant kinking, it must be deduced that compaction was a locally variable process restricted to certain parts of the cumulate pile, perhaps related to periods of greater crystal accumulation in the mush pile. When H is plotted against  $K_{mean}$  and CSD slope, no real relationship is observed in the former plot (Fig. 18a), although a weak positive trend is observed in the latter (Fig. 18b). This is important: although the values of  $K_{mean}$  indicate that the AMS fabrics are carried by magnetite, the strength of the fabrics would seem to be independent of the amount of magnetite present. We suggest that this indicates a pre-existing control on magnetite fabric formation; that is, the presence of a silicate template into which the magnetite crystallized. Magnetite is cumulus with plagioclase and clinopyroxene in the Druim Hain rocks, so we invoke an enhancement of magnetite growth in a certain direction as a result of simultaneous growth of minerals with higher aspect ratios, possibly during *in situ*

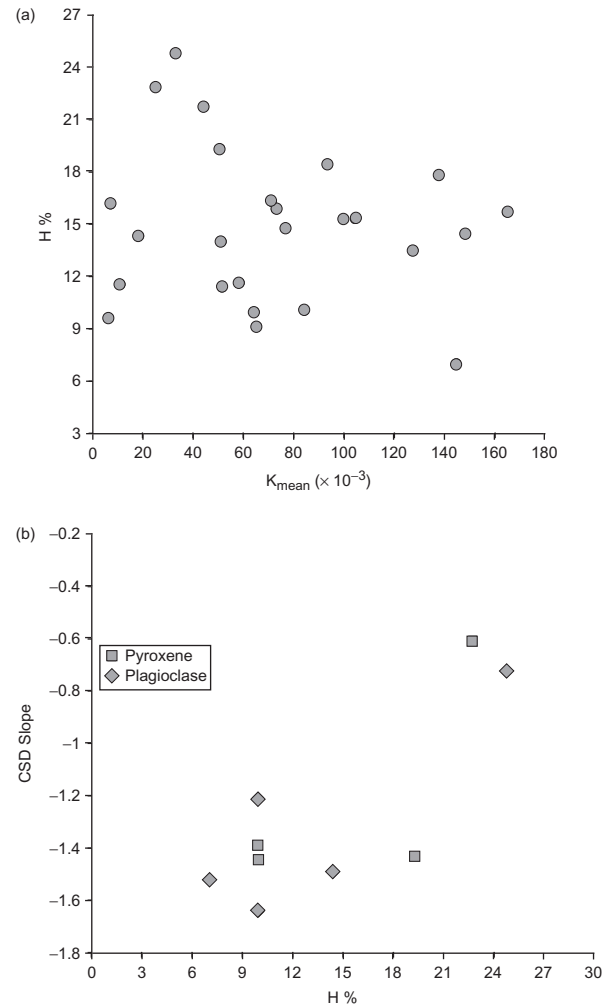


**Fig. 18.** Druim Hain layered gabbro plots of (a) H vs  $K_{mean}$  and (b) H vs CSD slope. (See text for discussion.)

crystallization as described above. Additionally, unlike Ardnamurchan, no evidence of obliteration of the fabric with increasingly shallower CSD slopes is observed; if anything, a positive trend is present, suggesting strengthening of H with increasingly shallow slopes. This reflects the textural observations that compaction-related deformation is observed in coarser-grained strongly foliated Samples 4, 15 and 23. If we take progressively shallow CSD slopes as reflecting increased Ostwald ripening (of the silicate framework), then this observation is in agreement with Boorman *et al.* (2004), who observed an increase in aspect ratio and strength of foliation intensity with increasing degrees of compaction. It is envisaged that this process [similar to the pressure-solution model of McBirney & Hunter (1995) and McBirney & Nicolas (1997), where the late growth of plagioclase in the cumulate pile is restricted to orientations parallel to the plane of lamination only] occurs in response to the effect the anisotropic distribution of melt pockets within the mush.

Our interpretation for the petrogenesis of the Druim Hain cumulates is thus based on placing the petrofabric and CSD observations in the context of the thin-section petrography. The combined dataset points to primary magma chamber processes being responsible for the initial development of the mineral lamination at Druim Hain; observation of grain boundaries and dihedral angles in most samples has shown that the textures appear to be unmodified impingement textures (i.e. showing little evidence of sub-solidus modification). In some samples, there are pockets of intercumulus material that contain well-rounded cumulus crystals; apparent dihedral angles in these cases approach values for melt-present equilibrium. Following localized compaction, minor textural readjustment in magnetite-rich samples at a late stage (as these features overprint compaction deformation features) formed the textures observed in Fig. 6g and h. As the magnetic foliation in all of the AMS samples consistently parallels the mineral lamination, it must be assumed that were there a consistent silicate lineation present, it would also be reflected by the magnetic fabric. It is possible that the overgrowth observed on magnetite cumulus crystals in the magnetite-rich samples may have affected the AMS lineations, if it occurred within lamination planes alone (as the magnetic foliations are not affected), and hence be responsible for the inconsistent magnetic lineations observed. However, overgrowth textures are not observed throughout the sample set, and magnetic lineations are inconsistent irrespective of the amount of magnetite present (and also in the intercept dataset). The lack of field evidence for magmatic flow (primary magmatic or mobilization of unconsolidated cumulate) is striking, as these features are common in well-layered intrusions, and this is also an important reason for attributing primary magmatic layer formation to *in situ* crystallization processes. It is also envisaged that a 400 m thick sequence of layers, such as at Druim Hain, would have contained excellent deformation marker horizons, were fluid dynamic processes or syn-magmatic deformation at layer boundaries (as has been inferred for the Ardnamurchan layered gabbros) important layer-forming processes. Indeed, the attitude of layer planes in the Druim Hain cumulates illustrates this, in part, by picking out the steepening inward of magmatic layer and lamination planes eastward, suggesting that some late central sagging may have occurred. This central sagging probably thus affected relatively coherent layers of cumulate, capable of undergoing such rotation without significant syn-magmatic disaggregation or deformation.

## CONCLUSIONS

### **Ardnamurchan laminated gabbros**

It is envisaged that an originally horizontal to sub-horizontal mineral lamination, developed synchronously

with localized small-scale magmatic layering, was rotated progressively inwards, giving rise to the syn-magmatic deformation observed and the consistent centrally plunging plagioclase and magnetite lineations on lamination planes. The consistency of these lineations and the similarity to lineations observed in the surrounding Great Eucrite gabbros by O'Driscoll *et al.* (2006), as well as the presence of syn-magmatic deformation structures, suggest that shearing and stretching (accompanying sagging) of unconsolidated cumulate was the dominant process responsible for mineral lamination formation. Combined petrographic and (plagioclase) CSD evidence indicates (in general) relatively simple textural evolution in the crystal mush, apart from the reorientation of grains described above. Zonation in plagioclase crystals from a single sample suggests a complex growth history, possibly indicating that the crystals were aggregated together from different locations in the magma chamber, prior to postcumulus overprint. There is also evidence, however, for sub-solidus textural modification, and the data would seem to suggest an accompanying (subtle) degradation of the fabrics observed. A slightly more protracted postcumulus crystallization history and textural evolution for the rocks of the (probably older) outer Sithean Mor laminated gabbro body may explain why not all of the lineations there conform to the dominant trend observed.

### **Druim Hain layered gabbros**

Field observations, combined with textural and magnetic fabric data, suggest that it is possible that the magmatic layering and mineral lamination of the Druim Hain Gabbros formed through *in situ* crystallization at the solidification front of an upward crystallizing mush zone. A lack of evidence of primary flow structures that can be attributed to 'magmatic sedimentation' at a crystal mush-magma interface indicates that such processes may have had a limited role in the development of mineral lamination. These observations correlate well with the petrofabric data, which suggest that the Druim Hain cumulates are not lineated. Our integrated dataset also provides evidence for localized postcumulus compaction. This is believed to have imposed crystal-plastic strain features on the textures of some samples, which otherwise reflect unmodified-inherited impingement textures. Minor overgrowth on cumulus magnetite crystals occurred following compaction. Late-stage central sagging of the Druim Hain cumulates, evidenced by the steepening inward (eastward) of the magmatic layering and mineral lamination, seems to have affected a relatively cohesive cumulate pile (i.e. one that cooled and largely solidified to too great an extent for syn-magmatic deformation to occur), thus in marked contrast to the situation in the Ardnamurchan laminated gabbros.

## ACKNOWLEDGEMENTS

John Reavy, Henry Emeleus and Brian Upton are thanked for field assistance and discussion, and Dougal Jerram for helpful observations on the crystal size distribution data. Constructive and thorough reviews by Marian Holness, Michael Higgins and Sandy Cruden considerably improved the quality of the paper. Funding from the Irish Research Council for Science, Engineering and Technology (IRCSET) is gratefully acknowledged by B.O'D. and from Science Foundation Ireland (SFI) by V.R.T.

## SUPPLEMENTARY DATA

Supplementary data for this paper are available at *Journal of Petrology* online.

## REFERENCES

- Archanjo, C. J., Bouchez, J. L., Corsini, M. & Vauchez, A. (1994). The Pombal granite pluton—magnetic fabric, emplacement and relationships with the Brasiliano strike-slip setting of NE Brazil (Paraíba State). *Journal of Structural Geology* **16**(3), 323–335.
- Ballet, O., Coey, J. M. D. & Burke, K. J. (1985). Magnetic properties of sheet silicates—2-1-1 layer minerals. *Physics and Chemistry of Minerals* **12**(6), 370–378.
- Balsley, J. R. & Buddington, A. F. (1958). Iron–titanium oxide minerals, rocks and aeromagnetic anomalies of the Adirondack area, New York. *Economic Geology* **53**, 777–805.
- Beausoleil, N., Lavallee, P. & Yélon, A. (1983). Magnetic properties of biotite micas. *Journal of Applied Physics* **52**, 906–915.
- Boorman, S., Boudreau, A. & Kruger, F. J. (2004). The Lower Zone–Critical Zone transition of the Bushveld Complex: a quantitative textural study. *Journal of Petrology* **45**, 1209–1235.
- Borradaile, G. J. (1988). Magnetic susceptibility, petrofabrics and strain. *Tectonophysics* **156**, 1–20.
- Borradaile, G. J. & Henry, B. (1997). Tectonic applications of magnetic susceptibility and its anisotropy. *Earth-Science Reviews* **42**, 49–93.
- Borradaile, G. J. & Jackson, M. (2004). Anisotropy of magnetic susceptibility (AMS): magnetic petrofabrics of deformed rocks. In: Martín-Hernández, F., Lunenburg, C. M., Aubourg, C. & Jackson, M. (eds) *Magnetic Fabric: Methods and Applications*. Geological Society: London, Special Publications **238**, 299–360.
- Bouchez, J. L. (1997). Granite is never isotropic: An introduction to AMS studies of granitic rocks. In: Bouchez, J. L., Hutton, D. H. W. & Stephens, W. E. (eds) *Granite: From Segregation of Melt to Emplacement Fabrics*, 8. Dordrecht: Kluwer Academic, pp. 95–112.
- Bouchez, J. L. (2000). Magnetic susceptibility anisotropy and fabrics in granites. *Comptes Rendus de l'Académie des Sciences, Série II, Fascicule a—Sciences de la Terre et des Planètes* **330**(1), 1–14.
- Boudreau, A. E. & McBirney, A. R. (1997). The Skaergaard Layered Series. Part III. Non-dynamic layering. *Journal of Petrology* **38**, 1003–1020.
- Bradshaw, N. (1961). The mineralogy and petrology of the eucrites of the Centre 3 igneous complex, Ardnamurchan, Scotland. PhD thesis, University of Manchester.
- Brothers, R. N. (1964). Petrofabric analysis of Rhum and Skaergaard layered rocks. *Journal of Petrology* **5**, 255–274.
- Cañon-Tapia, E. (1994). Anisotropy of magnetic-susceptibility parameters—guidelines for their rational selection. *Pure and Applied Geophysics* **142**(2), 365–382.
- Carr, H. W., Groves, D. I. & Cawthorne, R. G. (1994). The importance of synmagmatic deformation in the formation of the Merensky Reef potholes in the Bushveld Complex. *Economic Geology* **89**, 1398–1410.
- Cashman, K. V. & Marsh, B. D. (1988). Crystal size distribution (CSD) in rocks and the kinetics and dynamics of crystallisation II: Makaopuhi lava lake. *Contributions to Mineralogy and Petrology* **99**, 292–305.
- Collinson, D. (1983). *Methods in Rock Magnetism and Palaeomagnetism: Techniques and Instrumentation*. New York: Chapman and Hall.
- Constable, C. & Tauxe, L. (1990). The bootstrap for magnetic-susceptibility tensors. *Journal of Geophysical Research—Solid Earth and Planets* **95**(B6), 8383–8395.
- Coogan, L. A., Thompson, G. & MacLeod, C. J. (2002). A textural and geochemical investigation of high level gabbros from the Oman ophiolite: implications for the role of the axial magma chamber at fast spreading ridges. *Lithos* **63**, 67–82.
- Dunlop, D. & Özdemir, Ö. (1997). *Rock Magnetism*. Cambridge: Cambridge University Press.
- Emeleus, C. H. (1991). Tertiary igneous activity. In: Craig, G. (ed.) *The Geology of Scotland*, 3rd edn. London: Geological Society, pp. 455–502.
- Emeleus, C. H. & Bell, B. R. (2005). *British Regional Geology: The Palaeogene Volcanic Districts of Scotland*, 4th edn. Nottingham: British Geological Survey.
- Emeleus, C. H., Cheadle, M. J., Hunter, R. H., Upton, B. G. J. & Wadsworth, W. J. (1996). The Rum Layered Suite. In: Cawthorne, R. G. (ed.) *Layered Igneous Rocks*. Amsterdam: Elsevier, pp. 403–440.
- Ferré, E. C. (2002). Theoretical models of intermediate and inverse AMS fabrics. *Geophysical Research Letters* **29**(7).
- Ferré, E. C., Bordarier, C. & Marsh, J. S. (2002). Magma flow inferred from AMS fabrics in a layered mafic sill, Insizwa, South Africa. *Tectonophysics* **354**, 1–23.
- Fortey, N. J. (1980). Petrofabrics of laminated gabbros from the Centre 3 igneous complex, Ardnamurchan, Scotland. *Mineralogical Magazine* **43**, 989–994.
- Garrido, C. J., Keleman, P. B. & Hirth, G. (2001). Variation of cooling rate with depth in lower crust formed at an oceanic spreading ridge; plagioclase crystal size distributions in gabbros from the Oman Ophiolite. *Geochemistry, Geophysics, Geosystems* **2**, paper number 2000GC000136.
- Geikie, A. & Teall, J. J. H. (1894). On the banded structure of some Tertiary gabbros in the Isle of Skye. *Quarterly Journal of the Geological Society of London* **1**, 645–659.
- Graham, J. W. (1954). Magnetic susceptibility anisotropy, an unexploited petrofabric element. *Geological Society of America Bulletin* **65**(12), 1257–1258.
- Harker, A. (1904). The Tertiary Igneous Rocks of Skye. Memoir of the Geological Survey of the United Kingdom.
- Hext, G. R. (1963). Estimation of second-order tensors, with related tests and designs. *Biometrika* **50**(3–4), 353–373.
- Higgins, M. D. (1991). The origin of laminated and massive anorthosite, Sept Iles intrusion, Quebec, Canada. *Contributions to Mineralogy and Petrology* **106**, 340–354.
- Higgins, M. D. (1994). Numerical modelling of crystal shapes in thin-sections; estimation of crystal habit and true size. *American Mineralogist* **79**, 113–119.
- Higgins, M. D. (1998). Origin of anorthosite by textural coarsening: Quantitative measurements of a natural sequence of textural development. *Journal of Petrology* **39**, 1307–1325.
- Higgins, M. D. (2000). Measurement of crystal size distributions. *American Mineralogist* **85**, 1105–1116.
- Higgins, M. D. (2002a). The role of textural coarsening in the development of the Kigaplaik layered mafic intrusion, Labrador,

- Canada: a crystal size distribution study. *Contributions to Mineralogy and Petrology* **144**, 314–330.
- Higgins, M. D. (2002b). Closure in crystal size distributions (CSD), verification of CSD calculations, and the significance of CSD fans. *American Mineralogist* **87**, 171–175.
- Higgins, M. D. (2006a). Use of appropriate diagrams to determine if crystal size distributions (CSD) are dominantly semi-logarithmic, lognormal or fractal (scale invariant). *Journal of Volcanology and Geothermal Research* **154**, 8–16.
- Higgins, M. D. (2006b). *Quantitative Textural Measurements in Igneous and Metamorphic Petrology*. Cambridge: Cambridge University Press, 265 pp.
- Higgins, M. D. & Chandrasekharam, D. (2007). Nature of sub-volcanic magma chambers, Deccan Province, India: evidence from quantitative textural analysis of plagioclase megacrysts in the Giant Plagioclase Basalts. *Journal of Petrology* **48**, 885–900.
- Holness, M. B. (2005). Spatial constraints on magma chamber replenishment events from textural observations of cumulates: the Rum Layered Intrusion, Scotland. *Journal of Petrology* **46**, 1585–1600.
- Holness, M. B., Cheadle, M. J. & McKenzie, D. (2005). On the use of changes in dihedral angle to decode late-stage textural evolution in cumulates. *Journal of Petrology* **46**, 1565–1583.
- Holness, M. B., Nielson, T. F. D. & Tegner, C. (2007). Textural maturity of cumulates: a record of chamber filling, liquidus assemblage, cooling rate and large-scale convection in mafic layered intrusions. *Journal of Petrology* **48**, 1565–1583.
- Hrouda, F. (1982). Magnetic-anisotropy of rocks and its application in geology and geophysics. *Geophysical Surveys* **5**(1), 37–82.
- Irvine, T. N. (1980). Magmatic density currents and cumulus processes. *American Journal of Science* **280A**, 1–58.
- Irvine, T. N., Anderson, J. C. & Brooks, C. K. (1998). Included blocks (and blocks within blocks) in the Skaergaard intrusion: Geologic relations and the origins of rhythmic modally graded layers. *Geological Society of America Bulletin* **110**, 1398–1447.
- Jackson, M. & Tauxe, L. (1991). Anisotropy of magnetic-susceptibility and remanence—developments in the characterization of tectonic, sedimentary and igneous fabric. *Reviews of Geophysics* **29**, 371–376.
- Jelínek, V. (1978). Statistical processing of anisotropy of magnetic susceptibility measured on groups of specimens. *Studia Geophysica et Geodaetica* **22**, 50–62.
- Jelínek, V. (1981). Characterization of the magnetic fabric of rocks. *Tectonophysics* **79**(3–4), T63–T67.
- Jerram, D. A., Cheadle, M. J. & Philpotts, A. R. (2003). Quantifying the building blocks of igneous rocks: are clustered crystal frameworks the foundation?. *Journal of Petrology* **44**, 2033–2051.
- Launeau, P. & Cruden, A. R. (1998). Magmatic fabric acquisition mechanisms in a syenite: Results of a combined anisotropy of magnetic susceptibility and image analysis study. *Journal of Geophysical Research* **103**, 5067–5089.
- Launeau, P. & Robin, P.-Y. F. (1996). Fabric analysis using the intercept method. *Tectonophysics* **267**, 91–119.
- Liss, D., Hutton, D. H. W. & Owens, W. H. (2002). Ropy flow structures: A neglected indicator of magma-flow in sills and dikes. *Geology* **30**, 715–718.
- Marsh, B. D. (1988). Crystal size distribution (CSD) in rocks and the kinetics and dynamics of crystallisation I: Theory. *Contributions to Mineralogy and Petrology* **99**, 277–291.
- Marsh, B. D. (1998). On the interpretation of crystal size distributions in magmatic systems. *Journal of Petrology* **39**, 553–599.
- Martín-Hernández, F., Luneburg, C. M., Aubourg, C. & Jackson, M. (eds) (2004). *Magnetic Fabric: Methods and Applications*. Geological Society, London, Special Publications **238**.
- McBirney, A. R. & Hunter, R. H. (1995). The cumulate paradigm reconsidered. *Journal of Petrology* **103**, 114–122.
- McBirney, A. R. & Nicolas, A. (1997). The Skaergaard Layered Series: Part II. Dynamic layering. *Journal of Petrology* **38**, 569–580.
- McBirney, A. R. & Noyes, R. M. (1979). Crystallization and layering in the Skaergaard intrusion. *Journal of Petrology* **38**, 487–554.
- Meurer, W. P. & Boudreau, A. E. (1998). Compaction of igneous cumulates; Part II, Compaction and the development of igneous foliations. *Journal of Geology* **106**, 293–304.
- Mock, A. & Jerram, D. A. (2005). Crystal size distributions (CSD) in three dimensions: insights from the 3D reconstruction of a highly porphyritic rhyolite. *Journal of Petrology* **46**(8), 1525–1541.
- Morgan, D. J. & Jerram, D. A. (2006). On estimating crystal shape for crystal size distribution analysis. *Journal of Volcanology and Geothermal Research* **154**, 1–7.
- Morse, S. A. (1979). Kigaplait geochemistry I: Systematics, sampling and density. *Journal of Petrology* **20**, 555–590.
- Nicolas, A. (1992). Kinematics in magmatic rocks with special reference to gabbros. *Journal of Petrology* **33**, 891–915.
- O'Driscoll, B. (2007). The Centre 3 layered gabbro intrusion, Ardnamurchan, NW Scotland. *Geological Magazine* **144**(6), 897–908.
- O'Driscoll, B., Donaldson, C. H., Troll, V. R., Jerram, D. A. & Emeleus, C. H. (2007a). An origin for harrisitic and granular olivine from the Rum Layered Suite, NW Scotland: A crystal size distribution study. *Journal of Petrology* **2**, 253–270.
- O'Driscoll, B., Hargraves, R. B., Emeleus, C. H., Troll, V. R., Donaldson, C. H. & Reavy, R. J. (2007b). Magmatic lineations inferred from anisotropy of magnetic susceptibility fabrics in Units 8, 9, and 10 of the Rum Eastern Layered Series, Scotland. *Lithos* **98**, 27–44.
- O'Reilly, W. (1984). *Rock and Mineral Magnetism*. Glasgow: Blackie.
- Owens, W. H. (1974). Mathematical model studies on factors affecting the magnetic anisotropy of deformed rocks. *Tectonophysics* **24**, 115–131.
- Owens, W. H. (1994). Laboratory drilling of field-orientated block samples. *Journal of Structural Geology* **16**, 1719–1721.
- Owens, W. H. (2000a). Statistical analysis of normalised and unnormalised second-rank tensor data, with application to measurements of anisotropy of magnetic susceptibility. *Geophysical Research Letters* **27**, 2985–2988.
- Owens, W. H. (2000b). Statistical applications to second-rank tensors in magnetic fabric analysis. *Geophysical Journal International* **142**, 527–538.
- Owens, W. H. (2000c). Error estimates in the measurement of anisotropic magnetic susceptibility. *Geophysical Journal International* **142**(2), 516–526.
- Owens, W. H. & Bamford, D. (1976). Magnetic, seismic, and other anisotropic properties of rock fabrics. *Philosophical Transactions of the Royal Society of London* **283**, 55–68.
- Pearce, T. H. & Kolisnik, A. M. (1990). Observations of plagioclase zoning using interference imaging. *Earth-Science Reviews* **29**, 9–26.
- Pouchou, J. L. & Pichoir, F. (1984). A new model for quantitative X-ray microanalysis, Part I. Application to the analysis of homogeneous samples. *Recherche Aérospatiale* **3**, 13–38.
- Resmini, R. G. & Marsh, B. D. (1995). Steady-state volcanism, paleoeruption rates, and magma system volume inferred from plagioclase size distributions in mafic lavas; Dome Mountain, Nevada. *Journal of Volcanology and Geothermal Research* **68**(4), 273–296.
- Richey, J. E. & Thomas, H. H. (1930). The Geology of Ardnamurchan, North-west Mull and Coll. *Memoir of the Geological Survey of Scotland*. Edinburgh: HMSO.

- Rochette, P. (1987). Magnetic-susceptibility of the rock matrix related to magnetic fabric studies. *Journal of Structural Geology* **9**(8), 1015–1020.
- Rochette, P., Jackson, M. & Aubourg, C. (1992). Rock magnetism and the interpretation of anisotropy of magnetic-susceptibility. *Reviews of Geophysics* **30**(3), 209–226.
- Stevenson, C. T. E., Owens, W. H., Hutton, D. H. W., Hood, D. N. & Meighan, I. G. (2007a). Laccolithic, as opposed to cauldron subsidence, emplacement of the Eastern Mourne pluton, N. Ireland: evidence from anisotropy of magnetic susceptibility. *Journal of the Geological Society, London* **164**, 99–110.
- Stevenson, C. T. E., Owens, W. H. & Hutton, D. W. H. (2007b). Flow lobes in granite: the determination of magma flow direction in the Trarawagh Bay Granite, N. W. Ireland, using anisotropy of magnetic susceptibility. *Geological Society of America Bulletin* **119**, 1368–1386.
- Tarling, D. H. & Hrouda, F. (1993). *The Magnetic Anisotropy of Rocks*. New York: Chapman and Hall.
- Turner, S., George, R., Jerram, D. A., Hawkesworth, C. & Carpenter, N. (2003). Case studies of plagioclase growth and residence times in island arc lavas from Tonga and the Lesser Antilles and a model to reconcile discordant age information. *Earth and Planetary Science Letters* **214**, 279–294.
- Wager, L. R. & Brown, G. M. (1968). *Layered Igneous Rocks*. London: Oliver and Boyd, 588 pp.
- Wills, K. J. A. (1970). The inner complex of Centre 3, Ardnamurchan. BSc thesis, Royal School of Mines, University of London.
- Woodcock, N. & Strachan, R. (2000). *Geological History of Britain and Ireland*. Oxford: Blackwell Science, 423 pp.

## APPENDIX: THE ANISOTROPY OF MAGNETIC SUSCEPTIBILITY TECHNIQUE

### Introduction

The measurement of anisotropy of magnetic susceptibility (AMS) involves placing a sample in a low magnetic field that imparts no remanent magnetism to the sample. It is therefore induced magnetism that is measured and not remanent magnetism (or palaeomagnetism). The most important use of AMS is in the characterization, constraint and quantification of very weak or subtle mineral fabrics related to flow or tectonic deformation. It can also be used to study the emplacement direction of ignimbrites or lavas, palaeocurrent direction of sediments or incipient soft-sediment deformation. Publications by Graham (1954), Owens (1974, 2000c), Owens & Bamford (1976), Jelínek (1981), Hrouda (1982), Borradaile (1988) Jackson & Tauxe (1991), Rochette *et al.* 1992, Borradaile & Henry (1997), Bouchez (1997, 2000) and Borradaile & Jackson (2004) are a selection of important advances and reviews to which the reader is referred for further elaboration on this introduction. Key texts on rock magnetism and AMS include those by Collinson (1983), O'Reilly (1984), Tarling & Hrouda (1993), Dunlop & Özdemir (1997) and Martín-Hernández *et al.* (2004).

### AMS theory

A magnetic field causes a freely suspended bar magnet to rotate into alignment with it. This is due to induced magnetization. Atoms with unpaired electrons have a net magnetic moment in a particular direction, giving rise to a spontaneous magnetic field. External fields may induce a magnetization by reorienting this electron spin. The relationship between the strength of this response (the induced magnetization;  $M$ ) in the material and the strength of the applied field ( $H$ ) is the magnetic susceptibility ( $\mathbf{K}$ ):

$$M = \mathbf{K}H. \quad (1)$$

$\mathbf{K}$  is dimensionless and reported in SI units.

The variation of  $H$  with  $M$  describes the magnetic behaviour of a material. At the grain scale, the important classes of magnetic behaviours for most AMS studies (Fig. A1) are as follows.

(1) *Paramagnetism*. Paramagnetic grains have a positive proportional non-permanent relationship between  $H$  and  $M$ , even at high  $H$  strengths, and  $M$  is zero when  $H$  is zero (i.e. the magnetization is non-permanent) (Fig. A1a). This is exhibited by silicate minerals that contain Fe in their crystal lattice, such as ferromagnesian minerals, of which biotite is the most important. An important property of paramagnetism is that it is thermally disrupted, such that the susceptibility decreases with increasing temperature ( $T$ ) according to the Curie law (see Dunlop & Özdemir, 1997, p. 24) (Fig. A1b), where  $K_p \sim C/T$ ; the Curie constant ( $C$ ) being a measure of concentration and strength of the magnetic ions in a material.

(2) *Ferromagnetism*. Ferromagnetic grains have a strongly positive proportional relationship between  $M$  and  $H$ , but with a maximum value of  $M$  (saturation magnetization) (Fig. A1a). Although strictly not the same, 'ferrimagnetism' (the behaviour of magnetite) is often referred to as ferromagnetism (the behaviour of metallic Fe). Ferromagnetic grains may retain a remanent magnetization when subjected to a relatively high field. Ferromagnetic behaviour is almost always carried by magnetite in a rock, and is produced by the closely coordinated Fe ( $\text{Fe}^{2+}$  and  $\text{Fe}^{3+}$ ) cations. This coordination essentially inhibits the thermal disruption experienced by paramagnetic grains up to a certain temperature—the Curie temperature ( $T_c$ ), which for magnetite is  $\sim 580^\circ\text{C}$ . Below this temperature the susceptibility is constant, but above it ferromagnetic grains behave essentially paramagnetically according to the Curie–Weiss law (see Dunlop & Özdemir, 1997, p. 27) (Fig. A1b).

(3) *Diamagnetism*. This occurs in all materials but is generally overshadowed by even small amounts of paramagnetic and ferromagnetic grains.  $M$  has a slightly negative and non-permanent response to increasing  $H$ .

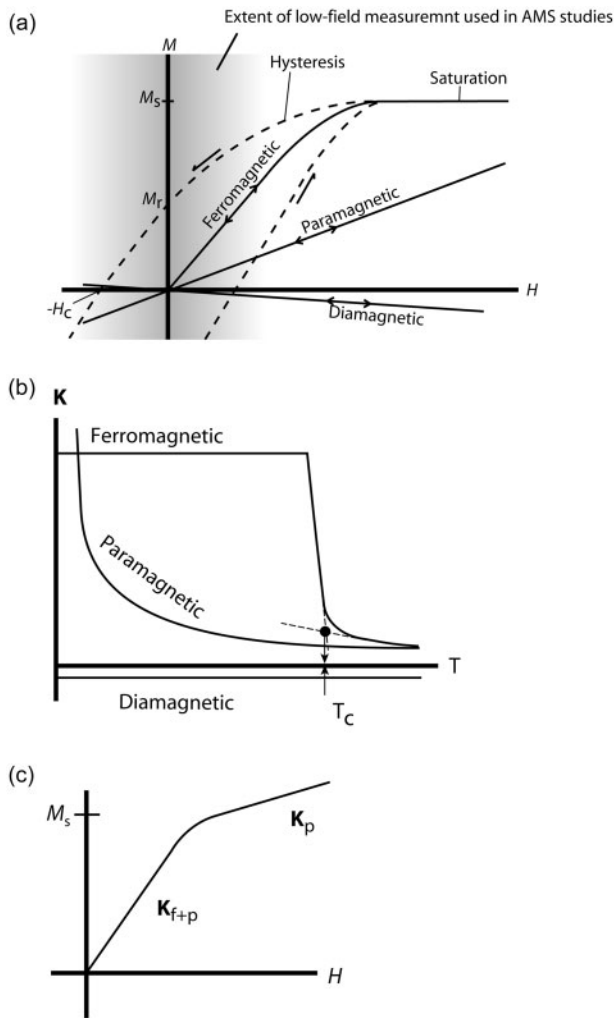


**Fig. A1.** (a) Sketch representing the main classes of magnetic behaviour according to  $M/H$ .  $M_r$ , remanent magnetization;  $M_s$ , saturation magnetization;  $H_c$ , coercive strength. (b) Relationship between  $K$  and temperature ( $T$ ). (c) In a sample with a combination of ferromagnetic and paramagnetic grains below the saturation magnetization field strength of the ferromagnetic grains,  $M/H$  = the sum of the paramagnetic grains' susceptibility ( $K_p$ ) and the ferromagnetic grains' susceptibility ( $K_f$ ). Once the ferromagnetic grains are saturated  $M/H = K_p$  alone.

### Factors controlling grain-scale AMS

There are several important differences in the way ferromagnetic and paramagnetic grains carry magnetic anisotropy. In ferromagnetic grains, Fe atoms are more closely coordinated and interact via intervening O atoms in magnetite. The coordination between Fe atoms means that the spin of electrons about neighbouring atoms is linked and is effectively the way in which a bar magnet is magnetized (a true ferromagnet). This results in pole surface charges and a demagnetizing field (Fig. A2), which gives rise to shape controlled anisotropy. Let us consider a needle-shaped grain; if magnetized along its long axis the

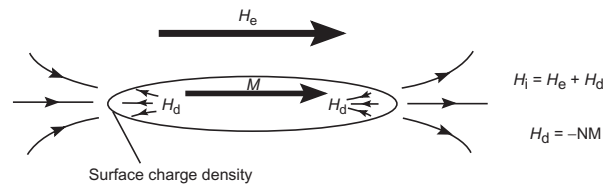


**Fig. A2.** The relationship between the grain shape, the induced magnetization and the demagnetizing field.  $H_i$ , induced field;  $H_e$ , external field;  $H_d$ , demagnetizing field;  $N$ , demagnetizing factor.

demagnetizing field is much less than if magnetized along one of its short axes. However, in very small grains ( $<0.1 \mu\text{m}$ ) the longest axis is actually the most difficult to magnetize and the shortest axis the easiest to magnetize, resulting in inverse anisotropy (see below).

The magnetic (principally Fe cation) atoms in paramagnetic grains are distributed throughout a silicate lattice in a non-interacting disordered arrangement. There is therefore no spontaneous or remanent magnetism in the grain. To reorient the electron spin direction of a Fe cation, the magnetic field must overcome the crystal lattice bond; the magnetic anisotropy is thus controlled mainly by the crystal lattice. Only in orthorhombic, tetragonal and trigonal crystal systems do magnetic principal axes correspond to crystallographic axes (Borradaile & Jackson, 2004; O'Driscoll *et al.*, 2007b). In Fe-bearing sheet-silicates, the most susceptible axis is usually within  $5^\circ$  of the  $a$ -axis and the least susceptible axis is similarly close to the  $c$ -axis (Borradaile & Henry, 1997; Borradaile & Jackson, 2004). This is because in biotite, Fe-Fe cation spacing is closer within the sheet-silicate layer than between layers, allowing effectively ferromagnetic coordination of Fe cations within silicate sheets (Beausoleil *et al.*, 1983; Ballet *et al.*, 1985). In other monoclinic minerals such as pyroxenes and amphiboles the magnetic axes do not correspond as closely to crystallographic axes and interpretation of AMS is somewhat more difficult (Borradaile & Henry, 1997).

The atomic coordination in ferromagnetic grains gives rise to sub-grain magnetic domains; this feature is important in explaining ferromagnetic behaviour and the size dependence of ferromagnetic grains on their anisotropic behaviour. In each sub-grain, the electron spins are parallel. The coordinated electron spins give rise to an internal magnetic field, which is equal to an external demagnetizing field (in the opposite direction) (Fig. A3a). A large external field is, however, energetically inefficient and the size of a single domain of parallel electron spins is limited to around  $0.1 \mu\text{m}$ . In grains larger than this, the coordinated electron spins divide themselves into domains divided by Bloch walls, arranged so as to minimize the external field (Fig. A3b).

In grains that are around  $0.1 \mu\text{m}$ , multi-domain (MD) behaviour may not be stable and the grain will exhibit some single domain (SD) behaviour (Fig. A3c); these are pseudo-single domains (PSD). Grains smaller than

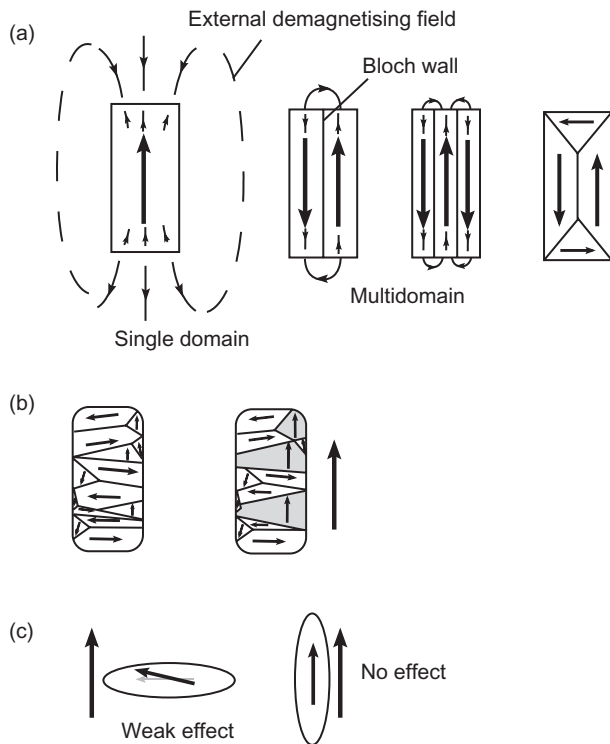


**Fig. A3.** (a) SD and MD configurations serve to minimize the external demagnetizing field. (b) Movement of the Bloch wall in MD grains gives rise to a magnetization when an external field is applied. (c) Inverse susceptibility anisotropy of a SD grain.

0.03  $\mu\text{m}$  are not large enough to retain coordinated magnetic moments and thus cannot retain magnetization and behave essentially paramagnetically. This is superparamagnetism (SPM) and is important for studies involving nanoparticles.

### Magnetic mineralogy

Diamagnetic materials, including the main rock-forming silicate minerals (quartz, feldspar and calcite), have an inherently weak magnetic response. Therefore a small proportion of paramagnetic grains ( $\sim 5$  wt %), and an even smaller amount of ferromagnetic grains ( $\sim 0.1$ – $1$  wt %), will dominate the susceptibility (Rochette, 1987; Tarling & Hrouda, 1993; Bouchez, 1997). In mafic igneous rocks, the AMS is almost certainly dominated by magnetite whether this is from a primary oxide phase or from inclusions in silicate minerals. Secondary magnetite (e.g. formed during low-temperature alteration) may also affect the AMS, either detrimentally to the fabric interpretation or beneficially (e.g. Stevenson *et al.*, 2007b). In felsic igneous rocks, paramagnetic and ferromagnetic grains can both be significant. In this case, it is desirable to differentiate the ferromagnetic and paramagnetic susceptibilities, although in most cases there is a correspondence between the ferromagnetic and the paramagnetic contributions

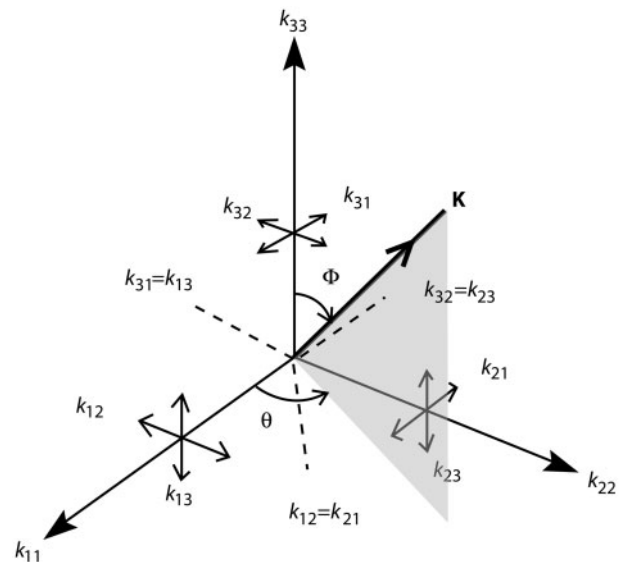


**Fig. A4.** The specimen axes relate to the susceptibility axes using standard coordinates in a Cartesian system. Assuming that the principal susceptibility axes are orthogonal, six tensor components are used.

(e.g. Archanjo *et al.*, 1994; O'Driscoll *et al.*, 2007b; Stevenson *et al.*, 2007b).

### Measurement

The magnetic susceptibility tensor is a second-rank tensor with three principal axes ( $K_1 \geq K_2 \geq K_3$ ) and corresponding principal axis directions. The specimen susceptibility tensor is

$$\mathbf{K} = \begin{bmatrix} k_{11} & k_{12} & k_{13} \\ k_{21} & k_{22} & k_{23} \\ k_{31} & k_{32} & k_{33} \end{bmatrix}. \quad (2)$$

(Owens, 2000b). The orientation of the principal susceptibility axes of the specimen is related to this matrix using conventional polar coordinates ( $\theta$  and  $\Phi$ ) in a Cartesian coordinate system by the equations

$$\begin{aligned} k_{11} &= (K_1 - K_3)\sin^2\theta\cos^2\Phi + K_3 \\ k_{22} &= (K_1 - K_3)\sin^2\theta\sin^2\Phi + K_3 \\ k_{33} &= (K_1 - K_3)\cos^2\theta + K_3 \\ k_{12} &= k_{21} = (K_1 - K_3)\sin^2\theta\sin\Phi\cos^2\Phi \\ k_{23} &= k_{32} = (K_1 - K_3)\sin\theta\cos\Phi\sin\Phi \\ k_{13} &= k_{31} = (K_1 - K_3)\sin\theta\cos\Phi\cos\Phi \end{aligned}$$

(Owens, 1974; see Fig. A4).

Results are reported for block averages of specimen AMS tensors, normalized by specimen mean susceptibility, on the assumption that the specimens from a sample or sampling station are representative of a homogeneous multinormal population. Detailed handling of the statistics

of anisotropy measurements has been described by Hext (1963), Jelínek (1981), Owens (1974, 2000*a*, 2000*b*, 2000*c*) and Constable & Tauxe (1990).

#### *AMS parameters*

The tensor may be visualized as an ellipsoid by giving each principal susceptibility axis a length. It is convenient to describe the ellipsoid with a set of parameters that together describe its size, shape and strength (or ellipticity). There are several parameter sets adopted in AMS studies, listed by Tarling & Hrouda (1993), Cañon-Tapia (1994) and Borradaile & Jackson (2004). Jelínek's (1981) widely used

$P_j$  (strength of anisotropy) and  $T$  (shape of ellipsoid) parameters, designed for strain analysis, involve the natural logarithm of the ratios of all three principal axes. This is suitable if anisotropies are large. However, the anisotropies measured in AMS studies of very weakly deformed rocks (particularly igneous rocks) are often of the order of a few per cent. The parameters adopted in this study (see Owens, 1974, and the main text) are based on the differences between the principal axes and are therefore more appropriate in describing very weak, as well as strong anisotropies (Owens, 1974, 2000*b*; Stevenson *et al.*, 2007*b*).